2011

A Study on the Miniaturization of Microstrip Square Open Loop Resonators

Luis Manuel Ledezma
University of South Florida, ledezmaluism@gmail.com

A Study on the Miniaturization of Microstrip Square Open Loop Resonators

by

Luis M. Ledezma

A thesis submitted in partial fulfillment
of the requirements for the degree of
Master of Science in Electrical Engineering
Department of Electrical Engineering
College of Engineering
University of South Florida

Major Professor: Thomas M. Weller, Ph.D.
Arthur D. Snider, Ph.D.
Lawrence P. Dunleavy, Ph.D.

Date of Approval:
May 13, 2011

Keywords: Microwave filters, surface mount capacitor, wide stop-band,
effective series resistance, quality factor

To Vanessa

Acknowledgments

It has been an honor to work throughout this project with Professor Thomas Weller, my academic advisor, whose knowledge about RF and microwave modeling and design never stopped amazing me, and who also is an excellent person. I would like to thank Dr. Larry Dunleavy for being part of my committee, and for being such a good boss at USF as well as at Modelithics. Thanks to Dr. Dave Snider, who not only accepted to be in my committee long after his retirement, but also for providing me with just-for-fun extra research opportunities. I am especially grateful to my mentor and friend Dr. Willie Moreno. He went beyond his duties to help me and my wife get established. The gratitude extends to his family; we have really felt like Moreno's adopted children and will be forever thankful for that.

This work would not be possible without the support of my wife Vanessa to whom this thesis is dedicated. There is not enough room to describe her role in my life and I shall not attempt it here. My family, and especially my parents and my parents in-law have, as well, blessed us with their support and encouragement. I must acknowledge the 412 crew and the Modelithics team for providing me with technical support. Special thanks to my friends Cristian Castro and David Cure who, despite stalling the writing of my thesis, provided the non-technical support that is always needed (even when not explicitly requested :). Finally, I am in debt to my undergraduate advisors Professors Alfonso Zozaya and Paulino Del Pino from the University of Carabobo in Venezuela; it is because of their influence that I decided to pursue graduate studies.

Table of Contents

List of Tables

List of Figures

Abstract

A miniaturization technique that allows the size of microstrip square open loop resonators to be reduced by more than 80% is presented and studied. The technique is based on the loading of the resonator with a series surface mount capacitor. It is shown that this technique allows the design of microwave bandpass filters with a wider stopband when compared with conventional designs. It is also proved that the insertion loss of the miniaturized filter is not degraded, but in fact can be maintained or even enhanced by the miniaturization process; this is true whenever the quality factor of the lumped capacitor is higher than the quality factor of the microstrip resonator. Finally, the feasibility of using the effect of the capacitor loss in the miniaturized resonator quality factor as a method to measure the effective series resistance of surface mount capacitors is studied, and recommendations towards its implementation are presented.

Chapter 1

Introduction

The miniaturization of electronic components has received a lot of attention in the last decades due to the rapid development of the telecommunication industry. Traditional high performance waveguide and dielectric resonator filters are usually too heavy and bulky for most applications like tower-top mounting in base stations [1]. This is also the case in satellite applications where payload costs are elevated, and high performance filters are usually needed. Lately, the accelerated market expansion of portable devices is pushing the needs for miniaturization to its limits. In most modern commercial products there is a very limited use for any large, high performance component. All this is stressed by the fact that most communication systems implemented nowadays operate below 6 GHz where distributed components are physically large.

Among all the filter technologies microstrip remains popular due to its ease of integration and compatibility with planar fabrication processes. Microstrip also favors miniaturization, it is light, and occupies low volume. Furthermore, electronically tunable and reconfigurable filters, like the notch filters employed in ultrawideband applications, can use surface mount varactors that are compatible with microstrip implementations [2]. The main disadvantage of microstrip resonators is the low quality factors usually obtained. However, for applications that require negligible insertion loss (like front ends of satellite receivers), or very narrow relative bandwidths, the ad-

vent of high temperature superconductors have rendered microstrip resonators with quality factors above 30,000 [1]. Moreover, the miniaturization levels achievable in microstrip can compensate for the size of the required cooling system producing overall transceivers that are smaller than conventional transceivers that use waveguide or dielectric resonator filters [1, 3].

The microstrip square open loop resonator is one of the most used structures for filter applications due to its compact size, of approximately $\lambda/8$ by $\lambda/8$, and versatility [4–7]. As a consequence of their popularity a great amount of work related to their miniaturization has been reported [8–16]. The most common structures are shown in Figure 1.1, along with the conventional square open loop resonator (Figure 1.1a).

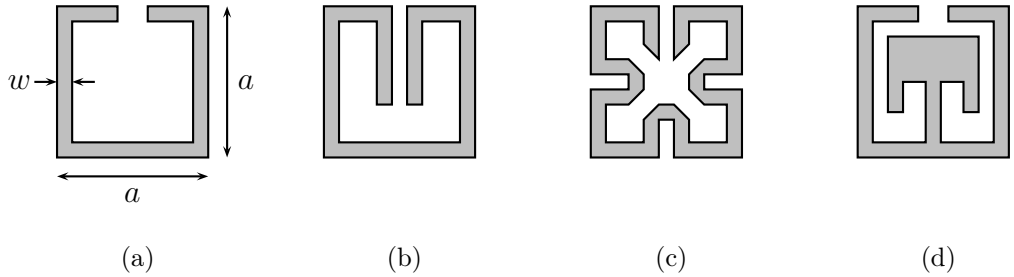

Figure 1.1: Square open loop resonator (SOLR) and some miniaturization techniques. (a) Conventional SOLR. (b) Folded arms SOLR. (c) Meander line SOLR. (d) Dual mode SOLR.

The origin of the folded arms square open loop resonator of Figure 1.1b can be traced back to the miniaturization of hairpin resonators [17]. As in the case of the meander line resonator of Figure 1.1c, the goal is to maintain a given physical length while occupying less total area by using the inner part of the resonator. In the case of the folded arms resonator the size is reduced more than what may be expected due to the coupling between the arms; the total area reduction is about 45% [17]. The folded arms can also be made of a lower impedance to increase the capacitance to ground improving the size reduction [10]. The resonator shown in Figure 1.1d saves real state

in a different way; it has two independent modes, and the coupling between them can be modified by the geometry of the inner structure. This dual mode resonator can then function as two independent resonators providing an immediate size reduction of 50%.

The method investigated in this research is the general case of loading the square open loop resonator with a series lumped capacitor as shown in Figure 1.2. This method has been used in the past with hairpin resonators and varactors to produce tunable filters [18]. Also, the miniaturization method proposed in [13] uses a structure that amounts to an interdigital capacitor connected as that shown in Figure 1.2. It is indeed surprising that in none of these two references a study of the general case of a lumped capacitor connected in series has been reported, even though such study may provide valuable insight into the properties, advantages, and limitations of related miniaturization methods.

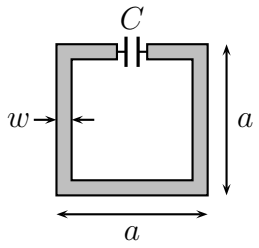

Figure 1.2: Square open loop resonator loaded with series lumped capacitor.

1.1 Thesis Contribution and Overview

The main objective of this thesis is to study the general case of the capacitively loaded microstrip square open loop resonator and its application to miniature microwave filter design. Towards this end the main theoretical background is covered in Chapter 2 where the behavior of the square open loop resonator is reviewed along with its properties relevant to filter applications such as the coupling between resona-

tors and its quality factors. In this chapter an error found in the literature regarding the estimation of the external quality factor of microstrip resonators is unveiled, and a corrected method is proposed. The chapter concludes with an exposition about the method used to synthesize microwave filters throughout this investigation.

The main contribution of this work lies in Chapter 3 where the theory and properties of the capacitively loaded resonators are explored in detail, including their characteristics as filter elements. Chapter 3 ends with the presentation of an example filter design that is 80% smaller than a conventional one, a miniaturization factor that is unattainable with previously reported methods. Moreover, the filter does not present a degradation in performance, but on the contrary, it has a lower insertion loss and wider spurious free stop-band.

In Chapter 4 the possibility to use the loaded square open loop resonator to measure some characteristics of the connected capacitor, like its effective series resistance and capacitance, is explored. Chapter 5 follows with a summary of conclusions and recommendations for future work.

Chapter 2

Theoretical Background

2.1 Introduction

To describe the behavior of narrowband bandpass filters three fundamental elements are necessary and sufficient [19]:

- Resonators tuned to a synchronous resonant frequency.
- Coupling between the resonators.
- Coupling from the first and last resonator to the external circuitry.

The resonators used in this investigation are microstrip square open loop resonators and their fundamental properties are studied in Section 2.2. Several aspects concerning the coupling between adjacent square open loop resonators are reviewed in Section 2.3. Section 2.4 is dedicated to the study the different quality factors that are important in the analysis of resonators and microwave filters. The chapter ends with a short review of modern microwave filter design given in Section 2.5 along with the method used in this research for synthesizing bandpass filters by computer optimization.

2.2 Square Open Loop Resonators

The microstrip square open loop resonator can be obtained by folding a straight open resonator as shown in Figure 2.1. Due to the corners and the fringing capacitance between the open ends, a rigorous calculation of the electromagnetic fields in the square resonator is impractical. However, it is possible to study the main characteristics of the resonant modes of the square open loop resonator by analogy to those of the straight resonator. This qualitative analysis can shed some light on the behavior of the resonator with minimum effort. The conclusions drawn using this approach can then be compared for validation against the actual distribution of the electromagnetic fields obtained with the aid of full wave simulators.

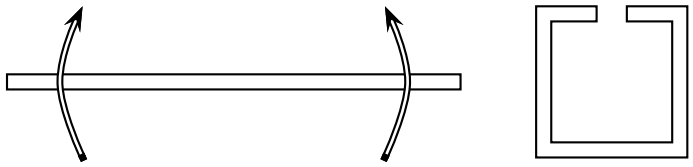

Figure 2.1: The square open loop resonator can be obtained by folding a straight open resonator.

Consider the straight microstrip open resonator shown in Figure 2.2a. The resonant frequency can be obtained by looking at the input admittance from any point within its length. Figure 2.2b shows an equivalent circuit that can be used to calculate this admittance as:

$$Y_{in} = jY_0 \left(\tan(\theta_1) + \tan(\theta_2)\right) = jY_0 \frac{\sin(\theta_T)}{\cos(\theta_1)\cos(\theta_2)} \tag{2.1}$$

where $\theta_T = \theta_1 + \theta_2$ is the total electrical length of the resonator. A standing wave can be maintained in the resonator whenever $Y_{in} = 0$. This yields infinite resonant

frequencies at:

$$\theta_T = n\pi \quad \text{or} \quad l = n\lambda/2 \tag{2.2}$$

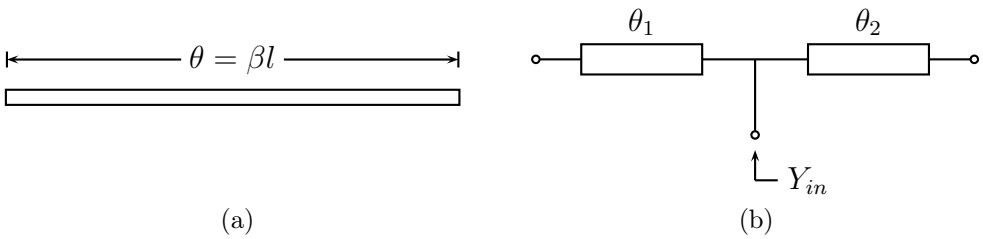

Figure 2.2: Microstrip open resonator. (a) Top view of a microstrip straight resonator. (b) Equivalent circuit used to calculate the input admittance from an arbitrary point within the length of the resonator.

The voltage distribution at the first two resonant frequencies ($n = 1, 2$) is shown in Figure 2.3. Since the open ends of the resonator force the current to be zero there, the voltage attains a maximum and the modes shown are the only ones allowed at those frequencies. If the loop were closed, this boundary condition would not apply and two orthogonal modes would exist at each frequency [20].

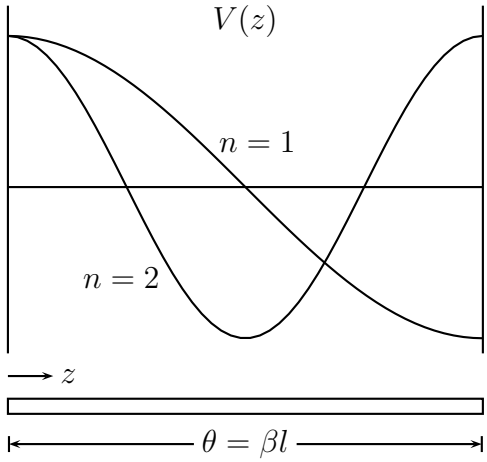

Figure 2.3: Voltage distribution in a straight open resonator.

When the denominator of Equation 2.1 is zero then $Y_{in} = \infty$ (or $Z_{in} = 0$). The positions where this occurs correspond to the voltage nulls in the mode diagram of Figure 2.3. At the first resonant frequency there is only one such null at $\theta_1 = \theta_2 = \pi/2$,

while at the second resonance there are two of them at $\theta_1 = \pi/2$ and $\theta_2 = 3\pi/2$. Knowing of the location of these voltage nulls is important since the resonator cannot be excited there. As an interesting consequence, by choosing carefully the feeding point of the resonator it is possible to excite only the odd (or only the even) modes of the resonator. Take, for example, the center of the resonator. At this point the fundamental resonance cannot be excited, nor can any other odd mode resonance. This observation translates to the square open loop resonator as is shown in Figure 2.4a.

Not all of the signature characteristics of a square open loop resonator can be obtained from the analysis of its straight counterpart. One of such is the possibility of exciting the resonator at both open ends at the same time as illustrated in Figure 2.4b. This feeding point will force an equal voltage on both open ends of the resonator. It can be seen in Figure 2.3 that the first mode of resonance (and actually all the odd modes) are characterized by opposite voltages at both ends, and hence they cannot be excited in this way.

(a) (b)

Figure 2.4: Two ways of exciting only the even modes of the square open loop resonator. (a) Excitation of the resonator in a null of the fundamental mode. (b) Excitation of the resonator symmetrically with respect to both open ends.

It is important to recall that the previous analysis was intended to show qualitatively the main characteristics of the square open loop resonator. Equation 2.2 may be used only to estimate the total length of a resonator, and in practice further tuning

has to be performed if a particular resonant frequency is desired. Two considerations that may help in the tuning process are:

- Reducing the gap between the open ends increases the effective length of the resonator more than expected due to the increase of the fringing capacitance across it.
- Meandering the corners reduces the effective length of the resonator increasing the resonant frequency.

The increase of the effective length of the resonator due to the increasing fringing capacitance across both open ends is of particular importance in this research and will be studied further in Chapter 3.

2.3 Coupling Between Resonators

The main interaction mechanism between resonators for filter applications is due to proximity coupling. This coupling can be characterized by a coupling coefficient that depends upon the ratio of coupled energy to stored energy as follows:

$$k = \frac{\int \varepsilon \boldsymbol{E_a} \cdot \boldsymbol{E_b} \, \mathrm{d}v}{\sqrt{\int \varepsilon E_a^2 \, \mathrm{d}v \int \varepsilon E_b^2 \, \mathrm{d}v}} + \frac{\int \mu \boldsymbol{H_a} \cdot \boldsymbol{H_b} \, \mathrm{d}v}{\sqrt{\int \mu H_a^2 \, \mathrm{d}v \int \mu H_b^2 \, \mathrm{d}v}} \tag{2.3}$$

where $\boldsymbol{E_a}$ and $\boldsymbol{H_a}$ are, respectively, the electric and magnetic fields produced by the first resonator, and $\boldsymbol{E_b}$, $\boldsymbol{H_b}$ are the corresponding fields of the second resonator.

The first term on the right-hand side of Equation 2.3 represents the coupling due to the interaction between the electric fields of the resonators, or more simply: the electric coupling. Similarly, the second term represents the magnetic coupling between the resonators. Depending on which term dominates the sum the coupling is said to be electric, magnetic, or mixed.

The nature of the coupling between square open loop resonators is related to the relative orientation of both resonators. Four canonical arrangements are shown in Figure 2.5. When the resonators are operating near their first resonant frequency, the pair of resonators depicted in Figure 2.5a interact mainly through their magnetic fields, this is because the magnetic field is maximum near the center of the resonator opposite to its open ends, maximizing the numerator of the second term of Equation 2.3. The configuration of Figure 2.5b produces, in turn, an electric coupling since the electric field is maximum near the open ends, maximizing the numerator of the first term of Equation 2.3. The coupling produced by the two configurations of Figures 2.5c and 2.5d are collectively referred as mixed coupling because neither the electric fields nor the magnetic fields dominate the interaction between the resonators.

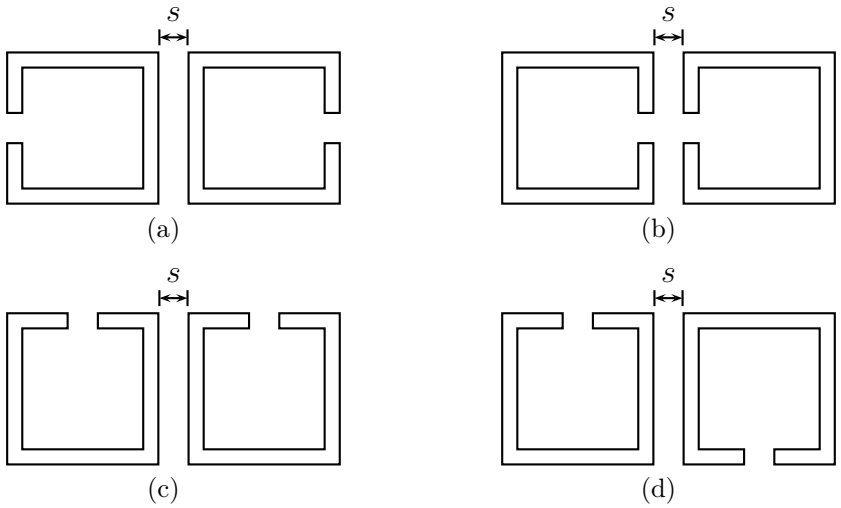

Figure 2.5: Typical arrangements of a pair of square resonators with (a) magnetic coupling; (b) electric coupling; (c) and (d) mixed coupling.

The definition of k given in Equation 2.3 is not practical for calculation purposes since it requires the knowledge of the electromagnetic fields everywhere. A useful alternative expression for k can be obtained from a well known fact in physics: when two resonators are coupled to each other they resonate together at two frequencies f_1 and f_2, that are, in general, different from their original resonant frequency f_0. Furthermore, these two frequencies are associated with two normal modes of oscillation of the coupled system, and their difference increases as the coupling between the resonators increases. A formula giving the exact relationship between these quantities is derived in [21] and is given by:

$$k = \frac{f_2^2 - f_1^2}{f_1^2 + f_2^2} \tag{2.4}$$

To find the coupling between a pair of resonators like any of those of Figure 2.5, they are excited with a pair of loosely coupled feed lines to obtain a transmission parameter $S_{21}(\omega)$ from which the two resonant frequencies f_1 and f_2 can be obtained. This procedure can then be repeated for several separations s between resonators in order to produce a design plot that gives k vs. s.

2.4 Quality Factor

The equivalent circuit of a resonator coupled to an external system is shown in Figure 2.6. The external circuit is modeled by its Norton equivalent with a system admittance Y_0; the resonator is modeled near resonance as an RLC shunt circuit; the coupling between both is modeled as a black box that transforms the impedance seen by the resonator to Y_{ex} as indicated in the figure.

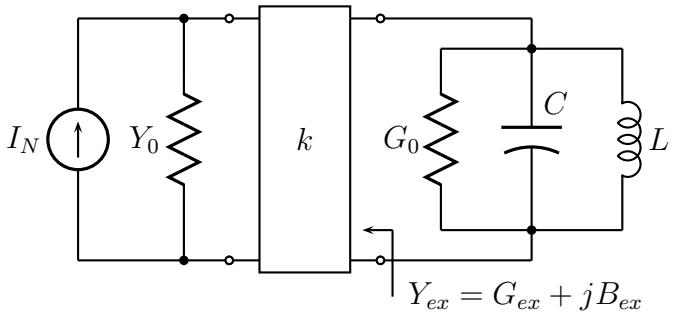

Figure 2.6: Equivalent circuit of a resonator connected to an external circuit. The coupling is modeled as a black box with coupling coefficient k.

The admittance Y_{ex} presented to the resonator affects the overall frequency response of the network. The reactive part (jB_{ex}) detunes the resonator changing f_0, while the conductance G_{ex} essentially impacts the quality factor. The change in f_0 depends heavily on the strength of the coupling and in many cases can be ignored. However, if the coupling is strong enough, the resonator may have to be retuned to obtain the desired resonant frequency.

The change in the quality factor due to G_{ex} is almost always important and can be quantified by an external quality factor defined as the quality factor of the system if the resonator were lossless:

$$Q_{ex} = \frac{\omega_0 C}{G_{ex}} \tag{2.5}$$

The actual quality factor that takes into account all the losses is called the loaded quality factor and is denoted by Q_L. It can be expressed as a function of the external and unloaded quality factors Q_{ex} and Q_0 as:

$$\frac{1}{Q_L} = \frac{1}{Q_0} + \frac{1}{Q_{ex}} \tag{2.6}$$

This is also the only quality factor that can be measured directly.

Another quantity of interest is the coupling coefficient between the resonator and the external circuit. This can be defined as the ratio between the power dissipated in the external circuit to the power dissipated within the resonator. Since the power is proportional to the conductance, and all the elements are in parallel in the model of Figure 2.6, this definition leads to:

$$k = \frac{P_{ex}}{P_0} = \frac{G_{ex}}{G_0} = \frac{Q_0}{Q_{ex}} \tag{2.7}$$

where k is the coupling coefficient. When $k = 1$ equal amounts of power are dissipated in the resonator and in the external circuit, and the coupling is said to be critical. If more power is dissipated within the resonator than outside it, k is less than unity and the coupling is said to be undercritical. In the opposite case the coupling is called overcritical. These last two cases are important in filter applications as explained below.

The unloaded quality factor of a resonator is one of its most important figures of merit since it determines the amount of loss associated with it. In order to determine Q_0 it is convenient to couple loosely ($k \ll 1$) with the measurement equipment. This is obvious after eliminating Q_{ex} from Equations 2.6 and 2.7, yielding:

$$Q_0 = Q_L(1 + k) \tag{2.8}$$

Hence, if k is small enough, the measured quality factor Q_L represents a good estimation of Q_0. In many cases either the coupling cannot be made small enough without exceeding some limitations of the measurement instruments, or a very accurate estimation of Q_0 is desired. In those cases a measurement approach that provides both Q_L and k should be followed. In the next section one such approach is outlined as well as some aspects that affect the unloaded quality factor of microstrip resonators.

In many filter applications the first and last resonators have to be tightly coupled to the rest of the system ($k \gg 1$). In this case these resonators are loaded in such a way that their resonant frequency changes and they have to be retuned. Since this retuning requires a modification of the geometry of the resonator, its unloaded quality factor is also changed. Because of this, it is better to have a method to find Q_{ex} directly instead of relying on a previously determined Q_0 and Equation 2.6. A method for calculating Q_{ex} along with a correction of an error found in the literature is presented in Section 2.4.2.

2.4.1 The Unloaded Quality Factor

The loss mechanisms affecting the quality factor of microstrip resonators are: conduction loss, dielectric loss, and radiation loss [22]. The overall quality factor can be expressed as a function of these as follows:

$$Q_0 = \omega_0 \frac{U}{P_T} = \omega_0 \frac{U}{P_c + P_d + P_r} \tag{2.9}$$

where Q_0 is the unloaded quality factor; U represents the energy stored in the resonator; P_T is the total power loss; P_c, P_d, and P_r are the power losses due to conduction, dielectric polarization, and radiation, respectively; and ω_0 is the resonant frequency. This expression can be also written as:

$$\frac{1}{Q_0} = \frac{1}{Q_c} + \frac{1}{Q_d} + \frac{1}{Q_r} \tag{2.10}$$

where the terms Q_c, Q_d, and Q_r represent the quality factor of the resonator due only to conduction, dielectric, and radiation losses, respectively. In some filter applications

the resonators are enclosed in metallic housings; in this case the radiation loss should be replaced by loss due to the conducting walls of the housing.

There exists a tradeoff between the different loss mechanisms and this guarantees the existence of maximum quality factor [23]. This maximum depends on the frequency, the dielectric and conductor materials used, the housing size (or the lack thereof), the substrate thickness, the conductor thickness and width, and so on; a quantitative study is better done using computer simulation, however, some general trends are obtained from basic physical principles: the higher the conductance of the conductors used, the higher Q_c will be; a thicker substrate will increase the value of Q_c and Q_d while increasing the radiation losses and producing possible unwanted coupling between resonators; a smaller dielectric constant increases Q_d but decreases Q_r and makes the structure bigger. For a given geometry and substrate, the conductor and dielectric loss dominate the unloaded Q at low frequencies while radiation does it at high frequencies, so there is a frequency where the unloaded Q is maximum [23].

The method used in this investigation to estimate Q_0 is based on the two port measurement setup depicted in Figure 2.7. When the coupling coefficients k_1 and k_2 are identical to each other the unloaded quality factor is [24]:

$$Q_0 = \frac{Q_L}{1 - |S_{21}(f_0)|} \tag{2.11}$$

The condition $k_1 = k_2$ is easy to achieve in computer simulations if the resonator has a plane of symmetry. In practice the mechanical tolerances may produce some error in the estimation of Q_0. Note that while the previous formula can be derived without assuming loose coupling, the accuracy is seriously reduced if the coupling is

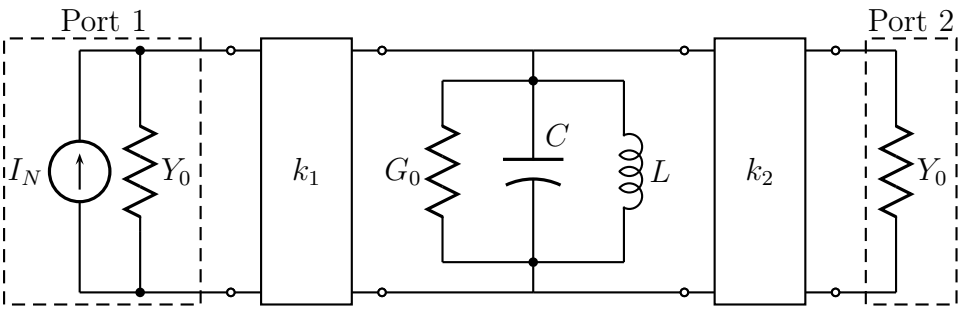

Figure 2.7: Two port measurement setup used to estimate the unloaded quality factor of a resonator.

tight since $|S_{21}(f_0)|$ would be close to 1 producing large errors in Q_0 even for small errors in Q_L. In practice a value of S_{21} at resonance of roughly $-30\,\text{dB}$ to $-40\,\text{dB}$ is considered loose enough [25].

2.4.2 The External Quality Factor

The coupling structure used for the input and output of filters throughout this research is shown in Figure 2.8. The external quality factor is controlled by the location of the tapped line t. When the tapped line is located at the center of the resonator, i.e. when $t = 0$, the external quality factor is very large since the resonator cannot be excited at that position. Increasing t gradually decreases the external quality factor.

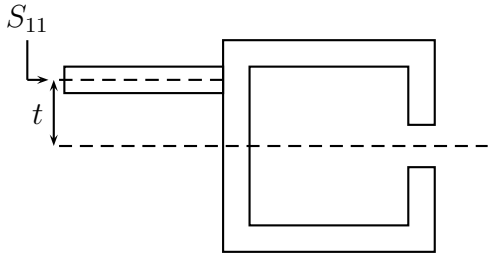

Figure 2.8: Tapped line structure used to couple to the first and last resonators of filters in this investigation.

In order to estimate Q_{ex} a one port measurement method based on the phase of S_{11} is proposed in [21]. The method relies on the fact that while the magnitude of S_{11} is almost constant near resonance (since the resonator behaves as an open circuit), the phase varies enough to be useful as a means to find Q_{ex}. Furthermore, by definition, the impedance of the resonator at resonance is real and thus the phase of S_{11} is zero. It is shown in [21] that the external quality factor can be expressed as:

$$Q_{ex} = \frac{f_0}{f_{-90^\circ} - f_{+90^\circ}} = \frac{f_0}{\Delta\omega} \tag{2.12}$$

where f_{+90° and f_{-90° are the frequencies at which the phase of S_{11} is 90° and -90°, respectively, and $\Delta\omega = f_{-90^\circ} - f_{+90^\circ}$. A plot of the phase of S_{11} showing these frequencies is shown in Figure 2.9.

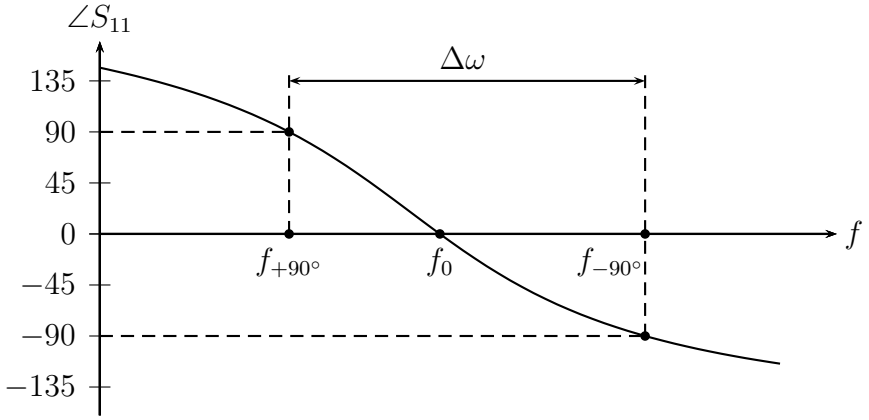

Figure 2.9: Phase of the reflection coefficient near resonance.

The previous formula was derived based on a lumped equivalent circuit that models the resonator as a shunt RLC circuit. If the reference plane used to measure S_{11} does not coincide with this equivalent model, then the method fails since the phase of S_{11} at resonance is not zero anymore.

To solve this issue the authors of [21] proposed to simply redefine f_{+90° and f_{-90° as the frequencies at which the phase shifts $\pm 90^\circ$ with respect to the absolute phase at f_0. Note that this is equivalent to assuming that the phase shift added by the

difference in reference planes is frequency independent, i.e., the phase plot is shifted up or down by a constant amount, but a shift in the reference plane can be modeled as the addition of a $50\,\Omega$ transmission line with fixed physical length between the resonator and the measurement plane. In this case, the time delay is constant and equals the change in the derivative of the phase of S_{11}.

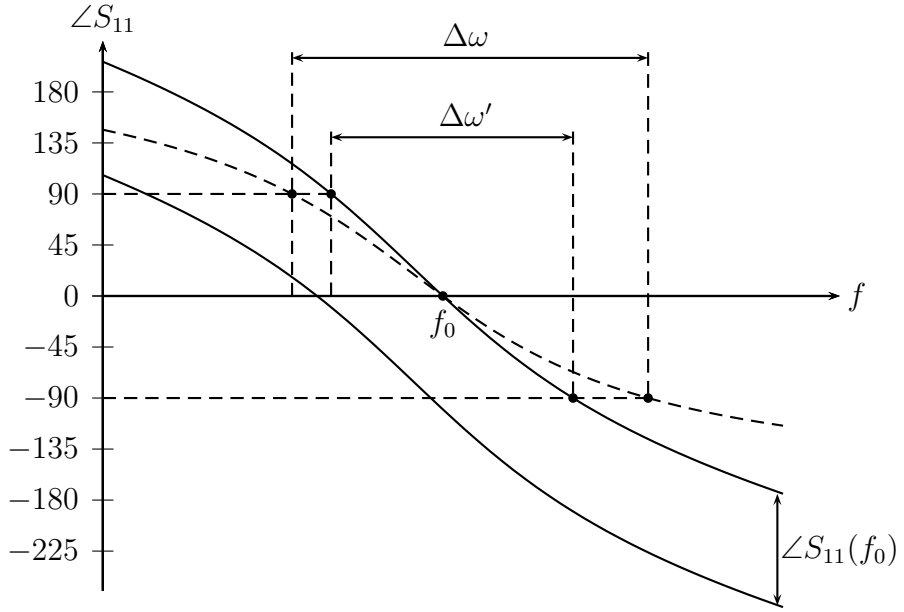

Figure 2.10: Phase of S_{11} with an extra time delay.

An illustration of this is presented in Figure 2.10. The dashed curve belongs to the resonator with the correct reference plane; the lower continuous curve is $\angle S_{11}$ of the same resonator when a different reference plane is used. The method suggested in [21] suggests that this curve be shifted upward until the phase at resonance is zero (see upper continuous curve) and then measure the bandwidth from f_{+90° and f_{-90°. This bandwidth has been denoted $\Delta\omega'$ in the figure and obviously differs from the original $\Delta\omega$ because of the change in the slope of $\angle S_{11}$.

In this investigation a new way to surpass this problem is proposed. The goal is to shift forward the reference plane using a transmission line with negative length

until the phase at resonance is zero. A schematic diagram of this approach is shown in Figure 2.11.

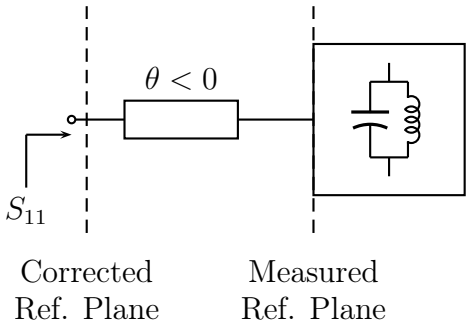

Figure 2.11: Proposed method to correct $\angle S_{11}$ using a transmission line with negative length to shift the reference plane.

Note that the amount by which the reference plane needs to be shifted forward is supposed to be unknown, otherwise the correction is trivial. In this case the condition $\angle S_{11}(f_0) = 0$ is only necessary but not sufficient since the reference plane could have been shifted initially more than 360°. This would produce several answers with $\angle S_{11}(f_0) = 0$ but with different slopes and thus, different estimations of Q_{ex}. The solution is to keep shifting the reference plane forward until a phase response with $\angle S_{11}(f_0) = 0$ and least slope is found without violating Foster's reactance theorem, this is, $\mathrm{d}\angle S_{11}/\mathrm{d}f$ should always remain negative.

The previous analysis is based on the assumption that $\angle S_{11}(f_0)$ is negative. In certain occasions this may not be the case and the reference plane has to be shifted backwards, i.e., the tranmission line added has to have positive electrical length. Physically this means that this extra transmission line is part of the resonant structure.

2.5 Bandpass Filter Design

Square open loop resonators are attractive for filter applications mainly due to their compact shape and diverse coupling mechanisms. The latter is particularly important in modern filter design where couplings with different signs between resonators within a filter may be necessary to obtain the desired response. This is the case in cross coupled filters where coupling between non-adjacent resonators can produce transmission zeros or flat group delay, depending on its sign.

The modern approach to the design of bandpass filters with n coupled resonators is based on the formulation of a coupling matrix of the form:

$$M = \begin{bmatrix} M_{11} & M_{12} & \cdots & M_{1n} \\ M_{21} & M_{22} & \cdots & M_{2n} \\ \vdots & \vdots & \ddots & \vdots \\ M_{n1} & M_{n2} & \cdots & M_{nn} \end{bmatrix} \tag{2.13}$$

where each element M_{ij} is proportional to the coupling between the i-th and j-th resonators. The coupling matrix is an $n \times n$ reciprocal matrix that along with the external quality factor of the first and last resonator uniquely describes the behavior of the filter.

Specifying the transfer response of a filter is thus equivalent, at least in principle, to specifying a coupling matrix and the external quality factors of the first and last resonators of the filter. The problem of obtaining the coupling matrix and external quality factors from a given filter response $S_{21}(\omega)$ is called synthesis; the inverse

problem of finding the response given the matrix and the quality factors is called analysis.

Many techniques have been devised to solve the synthesis problem, and it is still a very active area of research. The main difficulty is that most analytical techniques produce a fully populated coupling matrix that is impractical to implement. In this research, an approach based on computer optimization is used. The crux of the method is to generate a circuit representation of the coupling matrix and quality factors in order to perform optimization on it with a commercial circuit simulator.

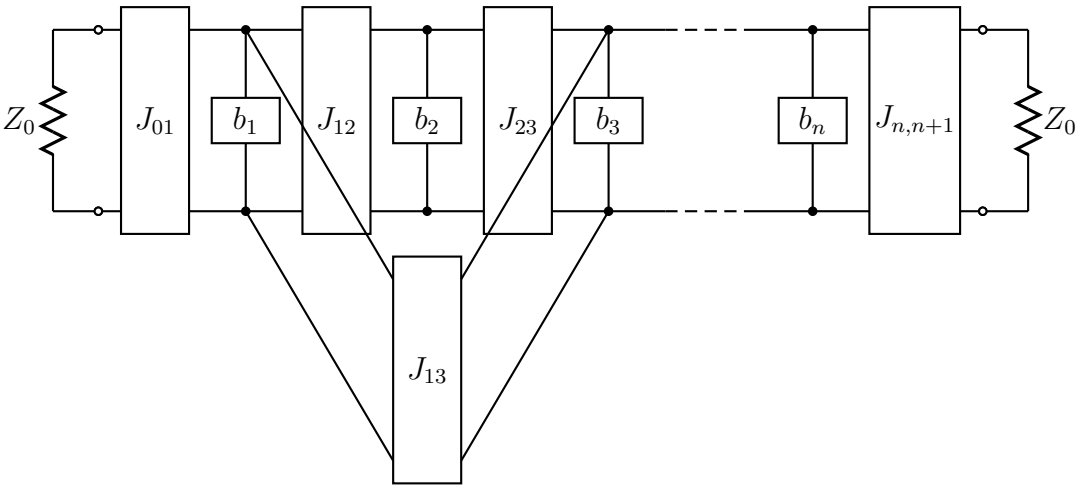

Figure 2.12: Generalized bandpass filter with admittance inverters and coupling between non-adjacent resonators.

Consider the general bandpass filter shown in Figure 2.12. The parameters b_1, b_2, $\ldots$, b_n are the susceptance slope parameter of the resonators, that is:

$$b_j = \frac{\omega_0}{2} \left. \frac{\mathrm{d}B_j(\omega)}{\mathrm{d}\omega} \right|_{\omega_0} \tag{2.14}$$

where $B_j(\omega)$ is the susceptance of the j-th resonator, and ω_0 is the resonant frequency.

The coupling between the i-th and j-th resonators is modeled with the admittance inverter J_{ij}. Note that this prototype includes coupling between non-adjacent resonators, e.g. resonators 1 and 3 are coupled through J_{13}. The relations between the susceptance slope parameters, the admittance inverters, the external quality factors, and the coupling factor between resonators are given by [26]:

$$Q_{e1} = \frac{b_1}{Z_0 J_{01}^2} \qquad Q_{e2} = \frac{b_n}{Z_0 J_{n,n+1}^2} \qquad M_{i,j} = \frac{J_{i,j}}{\sqrt{b_i b_j}} \tag{2.15}$$

where Q_{e1} and Q_{e2} represent the external quality factor of the first and last resonator, respectively.

The previous expression can be simplified further if some extra constraints are imposed on the filter. For instance, it may be required that all resonators be identical, this leads to:

$$b_1 = b_2 = \cdots = b_n = b \tag{2.16}$$

Also, a resonator may be modeled as a lumped RLC shunt resonator near its resonance frequency as illustrated in Figure 2.13a. In this case:

$$b = \omega_0 C = \frac{1}{\omega_0 L} \qquad \text{and} \qquad Q_0 = \frac{\omega_0 C}{G} = \frac{R}{\omega_0 L} \tag{2.17}$$

The last condition necessary to obtain an equivalent circuit is to determine an implementation for the admittance inverters. Since the model assumed for the resonators is already narrowband, nothing is lost if simple quarter wave transformers are used. If the characteristic impedance of the transformer that connects the i-th and

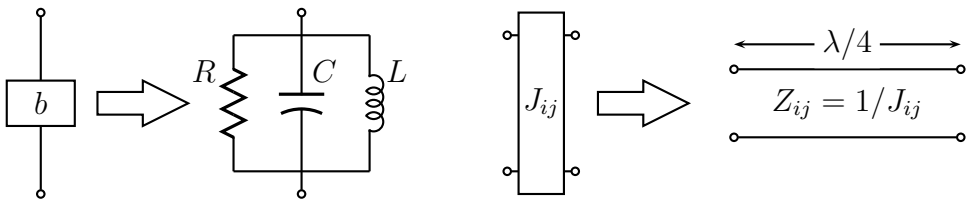

Figure 2.13: Models assumed for the components of the generalized filter. (a) A resonator is modeled as a lumped RLC shunt resonator. (b) An admittance inverter is modeled as a quarter-wave transformer.

j-th resonators is Z_{ij}, then:

$$J_{ij} = \frac{1}{Z_{ij}} \tag{2.18}$$

as depicted in Figure 2.13b.

Recall that the inclusion of impedance inverters increases the degrees of freedom on the filter parameters due to their impedance scaling property, therefore it can be assumed without lost of generality that:

$$J_{01}^2 = J_{n,n+1}^2 = \frac{1}{Z_0^2} \qquad \text{or} \qquad Z_{01} = Z_{n,n+1} = Z_0 \tag{2.19}$$

Combining the results 2.15-2.19 the following equations are obtained for the resonator parameters and quarter-wave transformers as a function of the unloaded quality factor of the resonators, the coupling between resonators, the external quality factor, the resonant frequency, and the system impedance:

$$R = Z_0 \frac{Q_0}{Q_e} \qquad C = \frac{Q_e}{\omega_0 Z_0} \qquad L = \frac{Z_0}{\omega_0 Q_e} \tag{2.20a}$$

$$Z_{ij} = \frac{Z_0}{Q_e M_{ij}} \quad i \neq 0 \text{ and } j \neq n+1 \tag{2.20b}$$

In summary, the synthesis process can be carried out as follows:

1. The unloaded quality factor of the resonators to be used is determined experimentally (or set to a high value if the losses do not need to be considered).

2. The desired topology is created in a circuit simulator using a structure like that shown in Figure 2.12 with the substitutions of Figure 2.13. The values of R, L, C, and Z_{ij} are given by Equations 2.20 with M_{ij} and Q_e as variables.

3. The parameters M_{ij} and Q_e are varied using an optimization algorithm until the desired response is obtained.

A final caveat: in some filter applications with cross coupled resonators the relative signs of the couplings is vital; often a coupling has to have a phase response opposite to that of the rest of the couplings, so it is said to be negative (though couplings actually have an absolute sign given by Eq. 2.3, in filter applications just the relative signs matter). Whenever a negative Z_{ij} is obtained from equation 2.20b this should be interpreted as a quarter wave transformer with characteristic impedance $|Z_{ij}|$ and electrical length $\theta = -90°$. This produces the desired phase response while maintaining a positive characteristic impedance.

Chapter 3

Miniature Microwave Filter

3.1 Introduction

The miniaturization of microwave filters below 3 GHz remains an active area of research due to the relatively large physical size of traditional resonators and the great demand from the wireless communication industry within this band. Square open loop resonators allow for the design of compact filter realizations and are among the most popular planar structures nowadays. Since they are already small ($\sim \lambda/8 \times \lambda/8$) further miniaturization is challenging. Common techniques to achieve miniaturization include loading the resonators with capacitively coupled lines [17], and meandering the lines [8]. Recently, dual mode resonators have been introduced that allow for an area reduction of nearly 50% [14].

In this chapter an aggressive miniaturization technique is introduced that allows the design of narrowband filters with an area reduction of about 80%. The technique is based on loading the square open loop resonator with a series lumped capacitor. This will be shown to result, not only in a smaller size, but also in a wider stop band.

3.2 Capacitively Loaded Resonator

The resonator proposed in this research is a microstrip square open loop with a lumped capacitor connected across its open ends as shown in Figure 3.1a. It will be shown in this section that this arrangement leads to miniaturization as well as other advantages over the square open loop resonator alone. A simple circuit model of the loaded resonator that will be used to derive its basic characteristics is shown in Figure 3.1b.

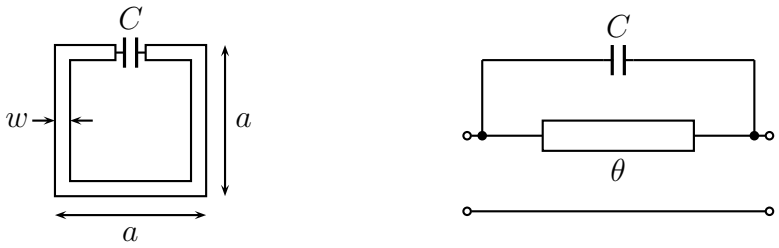

(a) (b)

Figure 3.1: Square open loop resonator loaded with a series capacitor. (a) Schematic representation. (b) Simple circuit model.

In order to apply a method similar to that used in Chapter 2 to derive the resonant condition of an open resonator, it is convenient to convert the model of Figure 3.1b to a more manageable one using Miller's theorem from electronics. In one of its many versions Miller's theorem states that the circuits of Figure 3.2a and 3.2b are equivalent if the following equations are satisfied:

$$Y_1 = Y(1-G) \tag{3.1a}$$

$$Y_2 = Y(1-1/G) \tag{3.1b}$$

where $G \equiv V2/V1$ is the voltage gain from node 1 to node 2, and it is supposed to be determined by independent means.

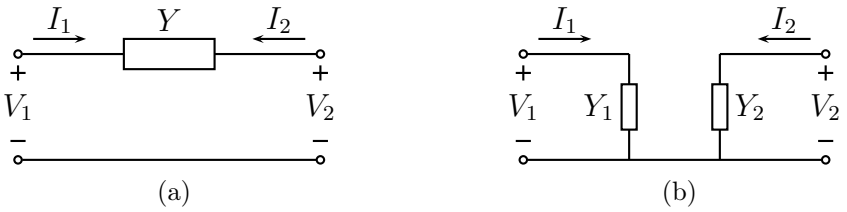

Figure 3.2: Miller's theorem. Circuits (a) and (b) are equivalent if Equations 3.1 are satisfied.

The goal is to apply this transformation to the circuit of Figure 3.1b in order to change the series capacitor to shunt capacitors connected between each open end and ground. This is illustrated in Figure 3.3a, where the shunt capacitors are assumed to have unknown values C_1 and C_2. To obtain these values, the ratio G between the voltage at both open ends is needed. This relation is, in general, not simple. Near resonance, however, it was shown in Chapter 2 that both voltages are in opposite phase and hence $G = -1$. Substituting this parameter in Equations 3.1 yields:

$$Y_1 = Y_2 = 2Y \qquad \text{or} \qquad C_1 = C_2 = 2C \tag{3.2}$$

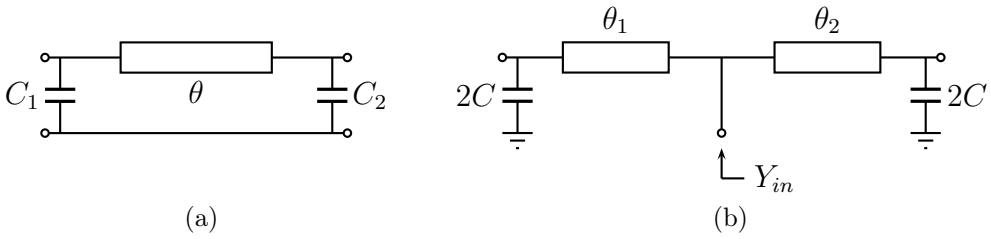

Figure 3.3: Equivalent circuit with two shunt capacitors at the open ends. (a) General case. (b) Near an odd mode resonance.

The condition for the fundamental resonance, therefore, can be found from the circuit shown in Figure 3.3b, by equating the input admittance to zero; this is:

$$Y_{in} = jY_0 \left[\frac{2\omega C + Y_0 \tan(\theta_1)}{Y_0 - 2\omega C \tan(\theta_1)} + \frac{2\omega C + Y_0 \tan(\theta_2)}{Y_0 - 2\omega C \tan(\theta_2)} \right] = 0 \tag{3.3}$$

After some manipulation and simplifications this equation can be casted into the simpler expression:

$$\tan(\theta_T) = \frac{4Z_0\omega C}{4Z_0^2\omega^2C^2 - 1} \tag{3.4}$$

where $\theta_T = \theta_1 + \theta_2$ is the total length of the resonator. This expression gives the electrical length necessary for resonance given a frequency and loading capacitance.

Note that after loading some properties of the square open loop resonator remain valid. In particular, it is possible to show that at the first resonant frequency the center of the resonator is a voltage null, i.e., a point where $Z_{in} = 0$. In effect, the condition for a voltage null is that the denominator of Y_{in} be zero, and when $\theta_1 = \theta_2$ this yields:

$$\tan(\theta_1) = \frac{1}{2Z_0\omega C} \tag{3.5}$$

When this equation is satisfied the center of the resonator presents a voltage null. However, recalling that $\theta_1 = \theta_T/2$ and the identity of the tangent of a double angle, it is easy to see that Equations 3.4 and 3.5 are equivalent. This means that whenever the resonance condition is satisfied there will be a voltage null at the center of the resonator. Moreover, Equation 3.5 may be used as the resonant condition instead of Equation 3.4.

Notice that the equivalent circuit of Figure 3.3b used to derive the resonant condition of the loaded resonator is valid only near an odd mode resonance, where the parameter G of the Miller theorem equals -1. Away from these frequencies the voltage relation among the open ends changes, and the equivalent admittances Y_1 and Y_2 do as well. This leads to great differences between the behavior of the series and shunt loaded resonators away from the odd resonant frequencies. The two most important

differences are the performance near the even resonant modes, and the existence of antiresonances in the case of series loading.

The circuit of Figure 3.3b has been studied previously in its own right, i.e. without any relation to the series loading, as a special case of a slow wave structure. The analysis done in the literature shows that the second resonance is also shifted down due to the capacitive loading [21]. In the case of the series loading shown in Figure 3.1b the situation is completely different; both open ends are in phase at even mode resonances so the capacitor is virtually open circuited (this can also be seen from the Miller theorem letting $G = 1$). Therefore, the series capacitor does not have any effect on the behavior of the resonator near even mode resonances; these resonant frequencies are unchanged by the presence of the capacitor.

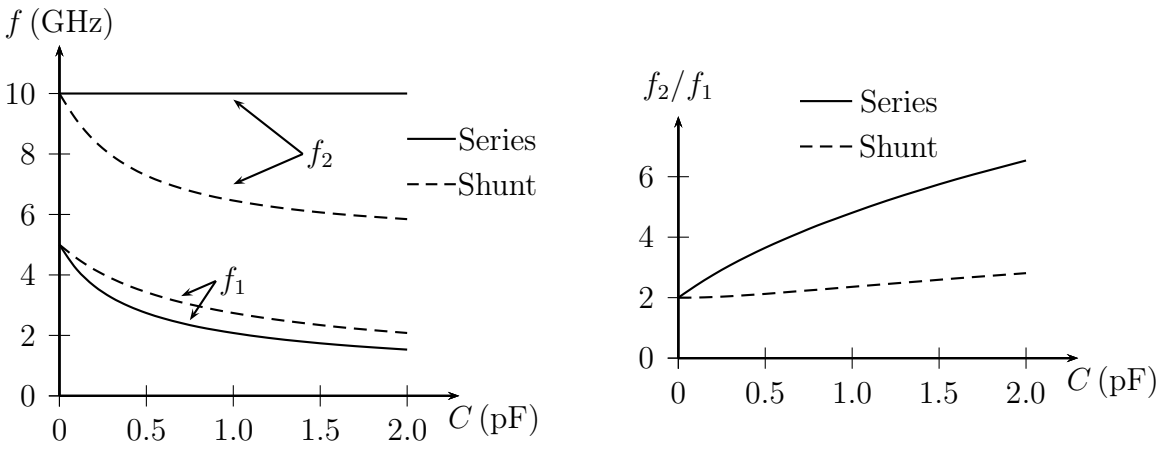

Figure 3.4: Resonant frequencies as a function of loading capacitance. (a) First and second resonant frequencies for series and shunt loading. (b) Ratio of the second to first resonant frequency for both cases.

As an illustration consider a microstrip open resonator with a characteristic impedance of 50 Ω, and fixed time delay of 0.1 nS (this is the ratio of the physical length to the velocity of propagation, both assumed to be constant). Figure 3.4a shows a plot

of the first and second resonant frequencies as a function of the loading capacitance for both, the series and the shunt cases. Note that since the second resonance is fixed in the series case, the distance between the first two resonances increases rapidly with the capacitance. To observe this more directly, a plot of the ratio f_2/f_1 is shown on Figure 3.4b. A greater ratio f_2/f_1 results advantageous for the design of bandpass filters with a wide stop band.

The results presented in Figure 3.4 are somewhat artificial since an ideal straight open resonator was used to generate them. The same experiment can be done with square open loops resonators using the set up shown in Figure 3.5. The parameter of interest is the transmission coefficient $S_{21}(\omega)$, where the resonant frequencies are manifested as peaks of maximum transmission between ports. Note that this and other experiments may be done by computer simulation, and they usually are.

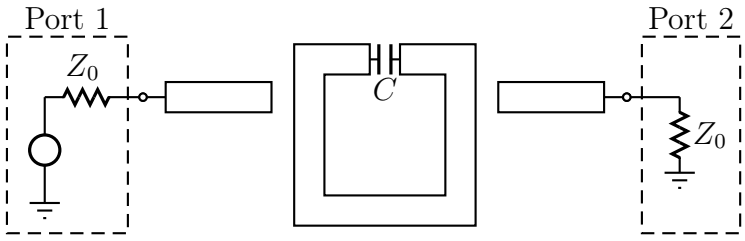

Figure 3.5: Setup used to measure the transmission coefficient $S_{21}(\omega)$. The distance between the resonator and the probes is not critical.

Figure 3.6 shows the result of this analysis obtained with the aid of a general purpose electromagnetic simulator [27], and with commercially available substrate dependent capacitor models [28]. The substrate used was RO4003c with a relative dielectric constant of 3.55 and a thickness of 60 mil (1.524 mm). In this case the size of the resonator is fixed with $\omega = 2\,\text{mm}$ and $a = 26\,\text{mm}$. The capacitors used belong to the ATC 600S 0603 family. Note how the first resonant frequency is shifted down with C while the second stays fixed. Note also that when the capacitance is increased

beyond certain value (1.4 pF in this specific example), a couple of frequencies where the transmission coefficient S_{21} is zero appear between the first and second resonant frequencies. This is observed in Figure 3.6 for the case with $C = 2\,\text{pF}$.

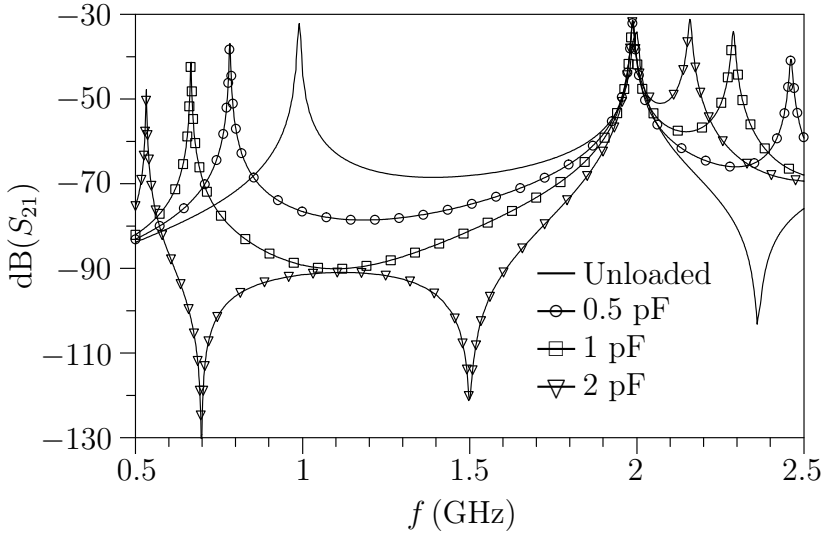

Figure 3.6: Transfer response of a capacitively loaded square open loop resonator for several capacitance values.

So far, the physical length of the resonator has been kept fixed while C is varied producing a shift in the first resonant frequency. This shift can be capitalized into miniaturization if we let the size of the resonator vary while we keep the fundamental resonance fixed. Table 3.1 shows a summary of the results obtained by fixing the resonant frequency at 1 GHz using the same substrate as before. In the table A_m denotes the area occupied by the miniaturized resonator while A_c represents the area of the conventional (unloaded) resonator. For simplicity the line width is $w = 2\,\text{mm}$ in all resonators. The quantity in the fifth row represents the ratio of the first spurious resonance frequency f_1 to the fundamental frequency f_0. Note that as the loading increases this ratio also does, e.g., when the loading capacitance is 1 pF the last row of Table I indicates that the area of the miniaturized resonator is 36% that of the conventional resonator (see fourth column), and that the first spurious resonance is at 3.54 GHz since $f_0 = 1\,\text{GHz}$ in this example.

Table 3.1: Resonator characteristics as a function of loading capacitance. The fundamental frequency is fixed at 1 GHz.

C(pF)	a (mm)	A_m(mm^2)	A_m/A_c	f_1/f_0
0	26	676	1	2
0.2	22.8	520	0.77	2.3
0.6	18.8	353.4	0.52	2.87
1	15.7	246.5	0.36	3.54

It is convenient to represent graphically the effect of the capacitive loading on the size of a square open loop resonator. In order to obtain a curve that represents the general trend of the area versus capacitance, two approximations will be done. In the first place it will be assumed that the total length of the square open loop resonator can be obtained from Equation 3.5, and hence:

$$\theta_1 = \frac{\theta_T}{2} = \frac{\beta l}{2} = \arctan\left(\frac{1}{2Z_0\omega C}\right) \tag{3.6}$$

where l represents the physical length of the resonator. The second approximation consists in neglecting the size of the gap where the capacitor is mounted, in this case l is the perimeter of the resonator and its area is given by:

$$A \approx \left(\frac{l}{4}\right)^2 = \frac{1}{16\beta^2}\theta_T^2 = \frac{1}{4\beta^2}\left[\arctan\left(\frac{1}{2Z_0\omega C}\right)\right]^2 \tag{3.7}$$

For a given substrate, line width, and frequency, the previous equation has the functional form:

$$A(x) = b\left[\arctan\left(\frac{1}{ax}\right)\right]^2 \tag{3.8}$$

where a and b are constant, and x is the capacitance. Since the constants a and b only have the effect of scaling the x and y axis respectively, any choice of them gives a good representation of the general tendency. A plot of this curve, where for simplicity $a = b = 1$, is shown in Figure 3.7a.

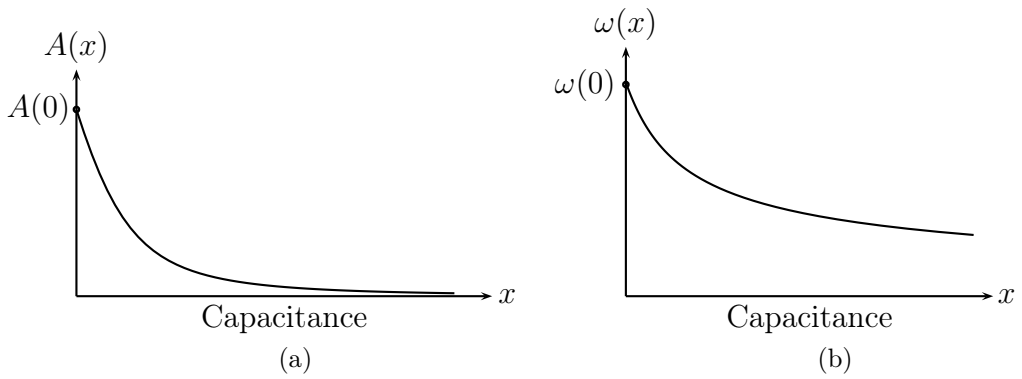

Figure 3.7: Relationship between the capacitance value and the resonator's area (a), and resonant frequency (b).

For a resonator with a fixed physical size, a curve showing the variation of the resonant frequency with the capacitance value is useful to determine the sensitivity to capacitor tolerances. The same approach used to generate Figure 3.7a can be employed with one caveat, the electrical length θ_T depends on frequency as well. Indeed, from Equation 3.5,

$$\tan\left(\omega\frac{l}{v_p}\right) = \frac{1}{2Z_0\omega C} \tag{3.9}$$

where v_p is the phase velocity. Although it is not possible to find an explicit expression for ω as a function of C, the inverse relationship is straightforward and can be written as:

$$x = \frac{a}{by\tan(by)} \tag{3.10}$$

where a and b are constants that depend on the substrate and resonator size, x is the capacitance, and y is the resonant frequency. This equation can now be plotted and inverted graphically. The result for $a = b = 1$ is shown in Figure 3.7b.

Both curves shown in Figure 3.7 indicate that there is maximum variability for relatively small values of capacitance (how small is small depends on the specific case, i.e. on the values of the constants a and b from previous equations). As the

capacitance increases the rate of change decreases. Some conclusions that can be drawn from this are:

- Designs with large capacitance values are more robust (less sensitive to capacitor tolerances).
- For tunable operation small values of capacitance are better.
- Increasing the capacitance after a certain value does not provide significant advantage.

Note that while large values of capacitance can provide robust designs, they may be unrealizable due to the small resonator area.

As a last aspect regarding the behavior of the series loaded open loop resonator, consider its voltage and current distribution. These can be derived at resonance using transmission line theory and the shunt equivalent model of Figure 3.3. This yields:

$$V(\theta) = \cos(\theta) - \frac{\sin(\theta)}{\tan(\theta_T/2)} \quad 0 < \theta < \theta_T \tag{3.11a}$$

$$I(\theta) = \frac{j}{Z_0}\left[\frac{\cos(\theta)}{\tan(\theta_T/2)} + \sin(\theta)\right] \quad 0 < \theta < \theta_T \tag{3.11b}$$

where $\theta = \beta z$ is the electrical length measured from one open end of the resonator, and θ_T is the total electrical length of the resonator. Figure 3.8 shows the plot of $V(\theta)$ and $I(\theta)$ as well as the voltage and current for the unloaded case (in dashed lines). Observe how the current never goes to zero but remains near its maximum value along the resonator and how the voltage varies almost linearly between open ends. A caveat: these plots are presented just to compare the distribution of the voltages and currents between the loaded and unloaded resonators, not their amplitudes; they

are normalized with respect to their respective maxima and they have either different frequencies or different resonator sizes.

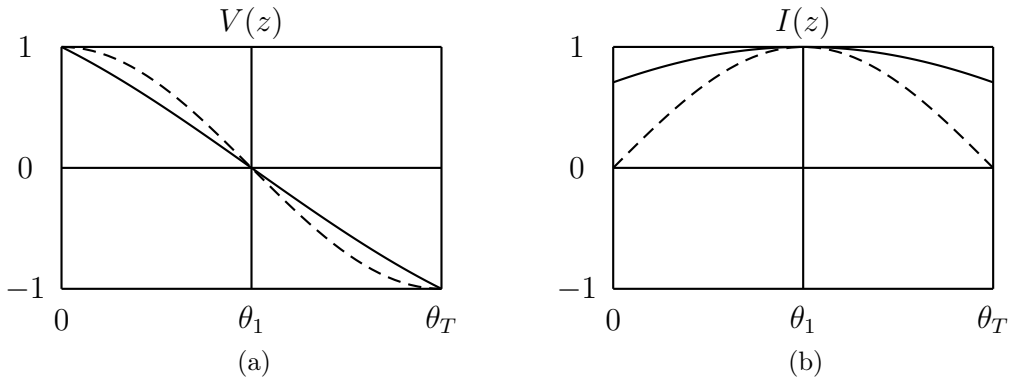

Figure 3.8: Voltage (a) and current (b) distribution in a loaded open loop resonator. Dashed lines are for the unloaded case.

3.3 Miniature Resonator as a Filter Element

The miniaturization of the square open loop resonator by the series capacitive loading proposed in the previous section affects some of its basic features. A study of the most important factors for filter applications has to be performed to guarantee that the resonator is still useful as a filter element. In this section the quality factor (both unloaded and external) of a miniature resonator and the coupling between resonators is studied. The study is done near the first resonant frequency since this is the most useful region for filter applications.

Probably the most fundamental difference between the conventional and the miniaturized resonator is the distribution of the electric field on them. While in both cases the electric field is mostly located near the open ends, in the miniaturized resonator most of the field is actually constrained to the interior of the capacitor. This has a major effect in both, the quality factor and the coupling between adjacent resonators.

3.3.1 Unloaded Quality Factor

The addition of the capacitor to the square open loop resonator changes its unloaded quality factor in two ways. First, the radiation losses from the open ends of the resonator are reduced increasing the quality factor of the resonator. Second, the capacitor dominates the losses due to dielectric polarization since most the electric field resides inside it. Therefore, a high Q capacitor could actually increase the unloaded quality factor of the whole resonator. This is analogous to the case of dielectric resonators where the fields are constrained to a small volume dielectric with high permittivity and low loss tangent resulting in a high overall Q.

To give a quantitative example of this effect, the quality factors of the resonators analyzed in last section were calculated and a column was appended to Table 3.1 as shown in Table 3.2. Note that the Q is higher for $C = 0.6\,\text{pF}$ and $C = 1\,\text{pF}$, in agreement with the previous discussion (the family of capacitors used in this research have quality factors on the order of 2000 near 1 GHz whereas the simulated microstrip resonator Q is about 230). The ability to decrease the size of a resonator while increasing or even maintaining its quality factor is not typical in microwave design. In this aspect this technique is unique. Observe that this advantage depends mainly on the capacitor having low losses, if another type of capacitor is used, e.g. interdigital, the quality factor may decrease with miniaturization.

Table 3.2: Resonator characteristics as a function of loading capacitance including the unloaded quality factor. The fundamental frequency is fixed at 1 GHz.

C(pF)	a (mm)	A_m(mm^2)	A_m/A_c	f_1/f_0	Q_u
0	26	676	1	2	234
0.2	22.8	520	0.77	2.3	220
0.6	18.8	353.4	0.52	2.87	240
1	15.7	246.5	0.36	3.54	269

3.3.2 Coupling Between Resonators

The miniaturization of the square open loop resonator reduces its capacity to couple to adjacent structures. This is expected since a smaller size represents a smaller volume of interaction between resonators; this is a common feature of any miniaturization technique. Probably the most special characteristic of the technique proposed in this research is the almost complete extinction of the electric coupling between resonators. This is due to the fact that the majority of the electric field that existed in the volume surrounding the open ends of a resonator is now confined to the interior of a capacitor limiting its possibility to interact with a neighboring resonator.

The effect on the magnetic and mixed coupling is less severe than for the electric coupling. An example is shown in Figure 3.9, where the magnetic coupling coefficient is plotted against the separation between resonators for different loading capacitors.

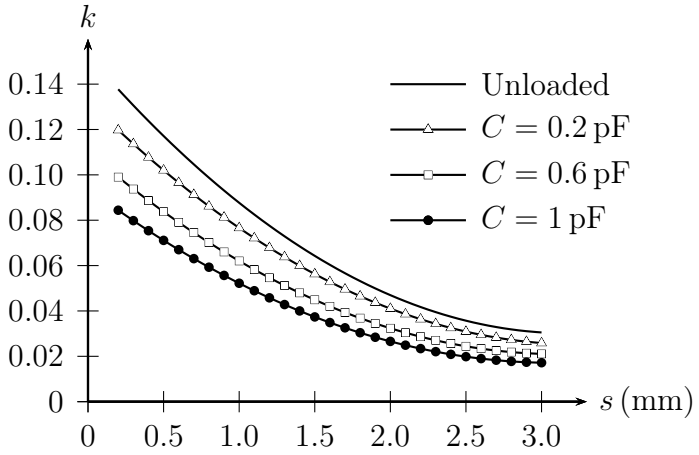

Figure 3.9: Magnetic coupling as a function of the distance between resonators for several values of the loading capacitor.

3.3.3 External Quality Factor

The external quality factor obtained by tapping into the resonator depends on the voltage level at the tapping point at resonance. It was mentioned in Chapter 2 that if the tapping point coincides with a voltage null, then no coupling is achieved between the resonator and the external circuit and the resulting quality factor is very large. Using the same reasoning, if the voltage at the tapping point is high then the external quality factor will be low. Referring to the voltage distribution of the conventional and the miniaturized resonator shown in Figure 3.8a, it is possible to predict that in the case of the conventional resonator the external Q will decrease rapidly as the tapping point is moved away from the voltage null at the center of the resonator. It is also evident from the figure that in the case of the miniaturized resonator the change in the external Q is slower. Therefore, the tapping distance from the null point necessary to obtain a given Q_{ex} is larger in the case of the miniaturized resonator.

Figure 3.10 shows the external quality factor of two different resonators, one conventional and one miniaturized, with the same resonant frequency (1 GHz). Note how the Q_{ex} diminishes quickly in the case of the unloaded resonator. Also note that in the case of the miniaturized resonator the plot is drawn for tapping points on the side of the resonator; this is because the quality factors obtained tapping closer to the null point produces large values of Q_{ex} that are difficult to estimate accurately.

3.4 Filter Example

As a proof of concept, four filters were designed having the same bandpass characteristic but with different degrees of miniaturization. The center frequency was chosen

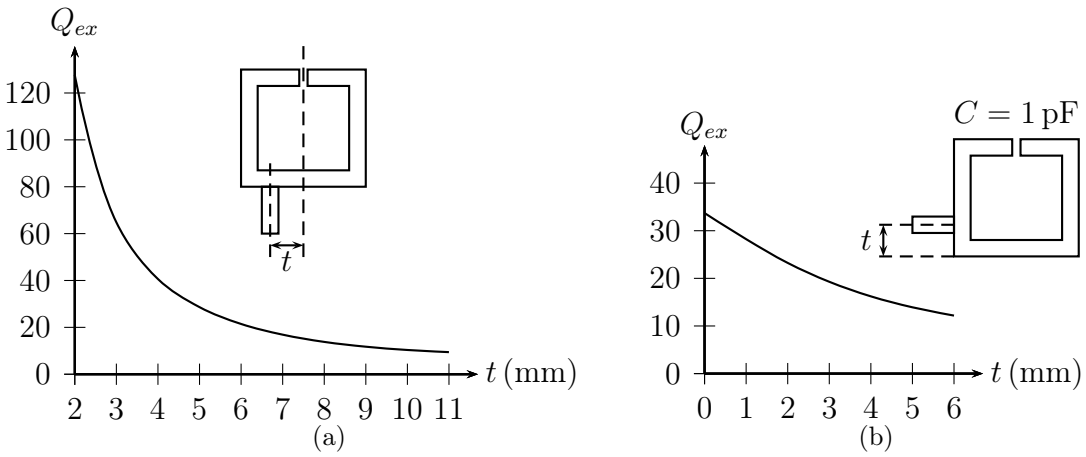

Figure 3.10: External quality factor of an: (a) unloaded resonator, and (b) a resonator loaded with $C = 1\,\text{pF}$ (b).

to be 1 GHz with a target bandwidth of 10%. A three pole equiripple response was used in all the cases. The first filter was not miniaturized and is used as a reference. Each resonator of the second filter was loaded with a low loss capacitor of nominal value 0.2 pF. The third and fourth filters were loaded with capacitors of 0.6 pF and 1 pF, respectively.

The layout of the four filters, including the dimensions for a substrate Rogers RO4003c ($\varepsilon_r = 3.55$) with a thickness of 60 mil (1.524 mm), are shown in Figure 3.11. The four filters are symmetrical with respect to a vertical line traced through the middle of the center resonator, i.e. the first and last resonators have the same dimensions. Note that the external coupling differs in all of the filters in order to obtain the necessary external quality factor Q_{ex}. In the four examples the size of the first and last resonator, as well as the distance between resonators, have been fine tuned to obtain an equiripple in-band return loss using a method similar to the one outlined in [25].

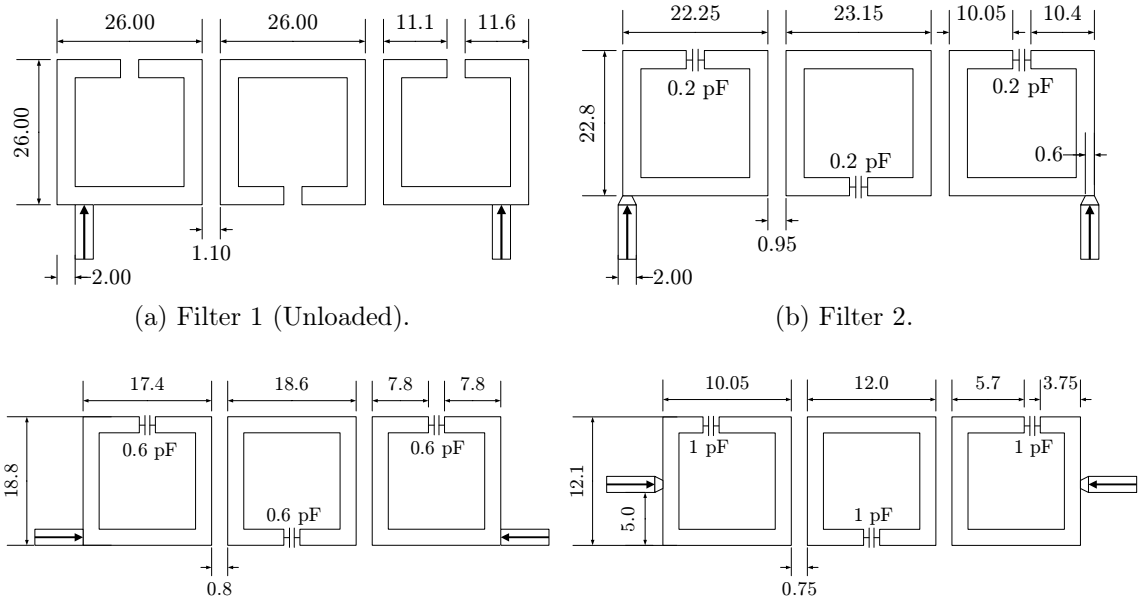

(a) Filter 1 (Unloaded).

(b) Filter 2.

(c) Filter 3.

(d) Filter 4.

Figure 3.11: Layout of the four filter examples (units are mm).

In Figure 3.12a the simulated broadband response of the four filters are compared, and the corresponding in-band response is shown in Figure 3.12b. Note that the four filters have similar response in the passband but differ considerably in the stopband. It can be also observed how the first spurious resonance is shifted towards higher frequencies for increasing degrees of miniaturization. In particular, the smallest filter does not present any spurious resonance in the frequency range shown.

A summary with the absolute and relative sizes of the designed filters is shown in Table 3.3. The last row represents the fraction of the area occupied by each filter relative to the area occupied by the first (non-miniaturized) one. Note that Filter 4 occupies an area equal to 20% that of the conventional design.

From these designs, Filter 1 and Filter 4 were built and measured. Figure 3.13 shows the broadband result of both filters. Observe that the spurious free stopband of the miniaturized filter extends beyond the frequency range considered as predicted

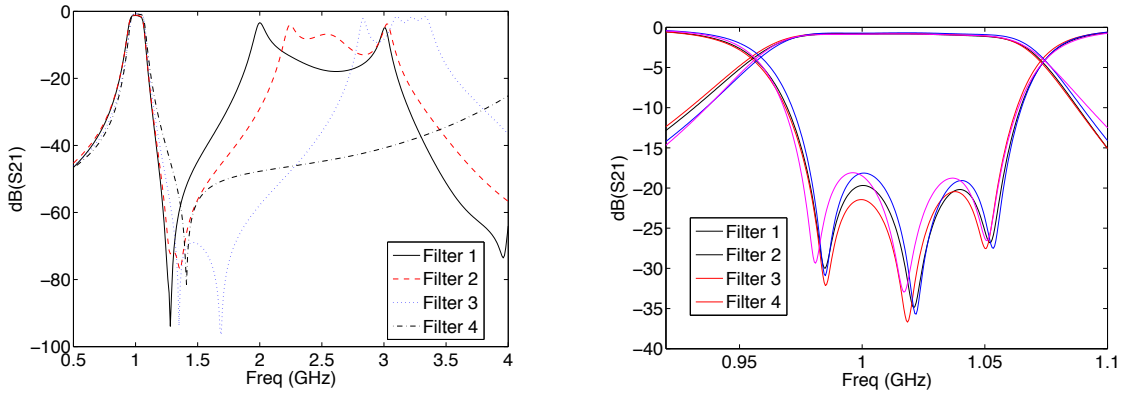

(a) (b)

Figure 3.12: Comparison of the simulated response of the four example filters. (a) Broadband response. (b) Passband response.

Table 3.3: Summary of relative and absolute sizes of the designed filters. The substrate used was RO4003c ($\varepsilon_r = 3.55$).

	Filter 1	Filter 2	Filter 3	Filter 4
Area (mm^2)	2033	1666	1034	407
A/A_1	1	0.82	0.51	0.20

by the simulations. Figure 3.14a shows the measured and simulated broadband response of the miniaturized filter (Filter 4). Note the general good agreement over the complete frequency range studied. Figure 3.14b shows the measured narrowband response versus the simulation. The shift in frequency of the miniaturized filter is mainly due to the tolerance of the capacitors and it represents the main disadvantage of this technique. Observe also that the insertion loss is basically the same for both filters.

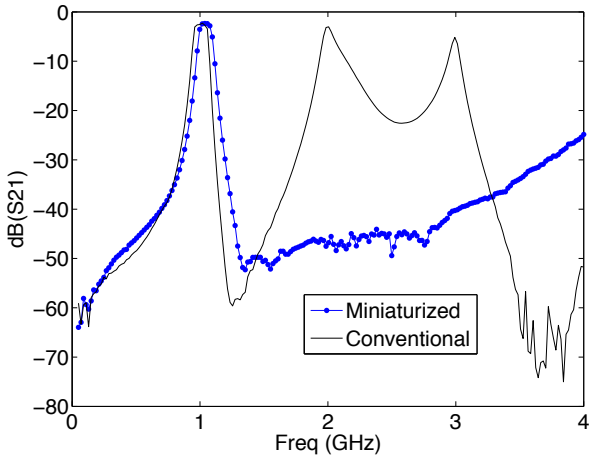

Figure 3.13: Measured broadband response of a conventional filter (Filter 1) and the proposed miniaturized design (Filter 4).

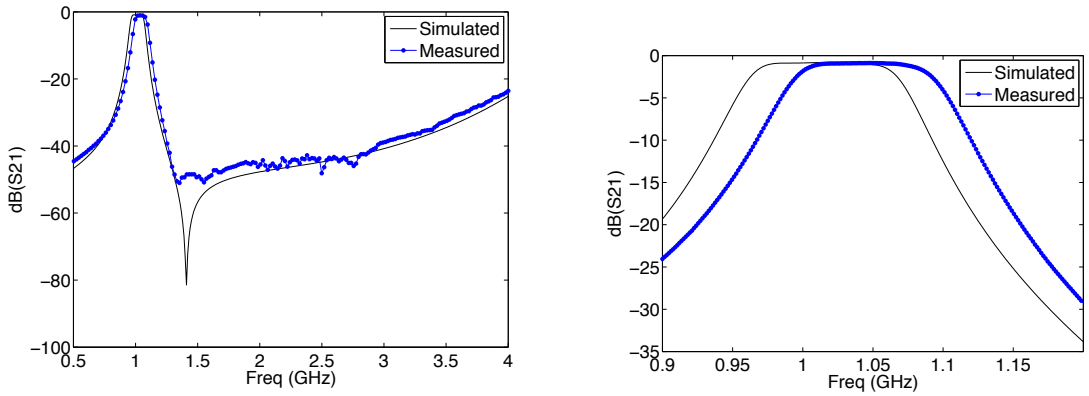

(a) (b)

Figure 3.14: Measured vs. simulated broadband response of the miniaturized filter.

Chapter 4

Measurement of Equivalent Series Resistance of Small Capacitors

4.1 Introduction

The equivalent series resistance (ESR) of a capacitor is an important modeling parameter that condenses the dielectric and conductor losses into a frequency dependent resistor. For many years the conventional method that has been used to measure the ESR of capacitors at microwave frequencies employs high-Q coaxial resonators as described in [29]; the setup is shown schematically in Figure 4.1. There are several potential error sources that limit the accuracy of this method for small capacitors with high Q, some of which are [30]:

- The parasitic capacitance between the inner conductor and the plunger. This capacitance increases when the size of the lumped component is decreased. Therefore, it can become comparable with the capacitor under test affecting the measurement. This effect may be safely ignored when the capacitor under test is large, both in size and in value.

- The transmission line discontinuity in the contact between the inner conductor and the lumped capacitor. This discontinuity adds inductance and resistance. If the part under test has low ESL and ESR, i.e. it is a high Q component with a high resonant frequency, then the discontinuity parasitics become comparable

with those of the part affecting the measurement accuracy. Again, usually if the capacitor is large the effect may be neglected.

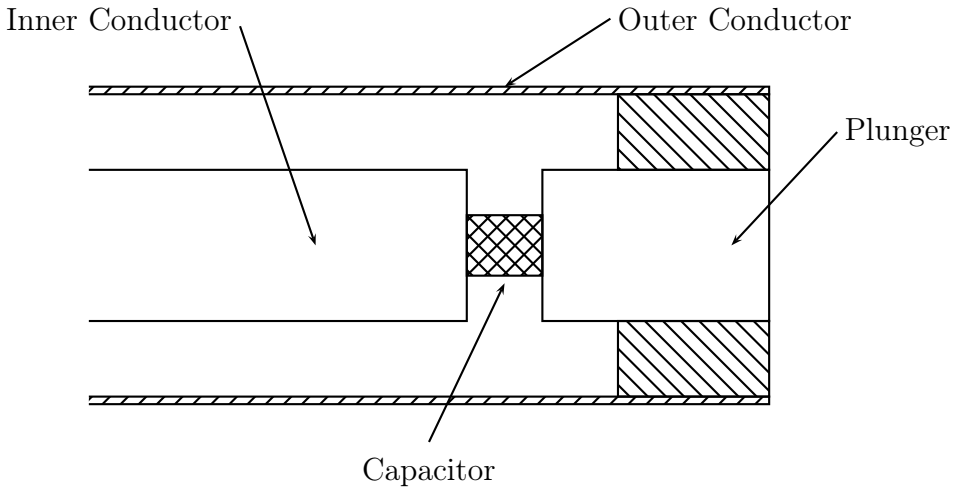

Figure 4.1: Standard method to measure ESR with a Boonton line.

In the miniature square open loop resonator introduced in the last chapter the ESR of the capacitor may have an important effect on the losses of the resonant structure. If this impact is large enough, then a square open loop resonator may be used to measure the ESR of small capacitors. The process may be described as simulation-based measurement and the general idea is illustrated schematically in Figure 4.2. First, an unloaded resonator is used to validate and calibrate the computer simulation. This step is crucial and without it the accuracy of any forthcoming measurement is unknown. The output of this step should be a computer simulation that closely matches the measurement throughout the desired frequency band.

The second step is to measure a similar resonator, i.e. with the same size, on the same substrate, and using the same VNA calibration, but loaded with a series capacitor. This situation can then be recreated in the computer just by adding the capacitor model to the previous calibrated simulation. The differences between the new simulation and measurement can be attributed to the capacitor model alone,

and an appropriate selection of the capacitor's parameters like capacitance, ESR, and ESL, should provide a close match to the measured data. These parameters can now be interpreted as "measured".

There are several drawbacks that limit the practical implementation of this method. The most important one is related to the first step since a match between the measured and simulated data may not be realizable to the desired degree of accuracy. This is especially true in the microwave range since many characteristics of the real system are idealized in the computer model. Such is the case of substrate parameters like its permittivity and loss tangent that are assumed constant with frequency and isotropic, as well as the conductor thickness, roughness, and cross section. Therefore, the initial step of matching the simulation and measurements to within a high degree of accuracy may require significant efforts and great amounts of time dedicated to modeling and measurements of the microstrip structure. Some of these requirements can be alleviated by the use of some specific substrates and fabrication processes with tighter tolerances.

The objective of this chapter is to investigate the effect of the capacitor ESR in the quality factor of the resonator. This will be done mainly in a simulation framework and may be used to provide an indication about the feasibility of the second step shown in Figure 4.2. For the reasons mentioned in the previous paragraph the actual implementation of this technique to measure the capacitor ESR falls outside the scope of this investigation. However, the insight gained through this study is used to generate recommendations towards its successful realization.

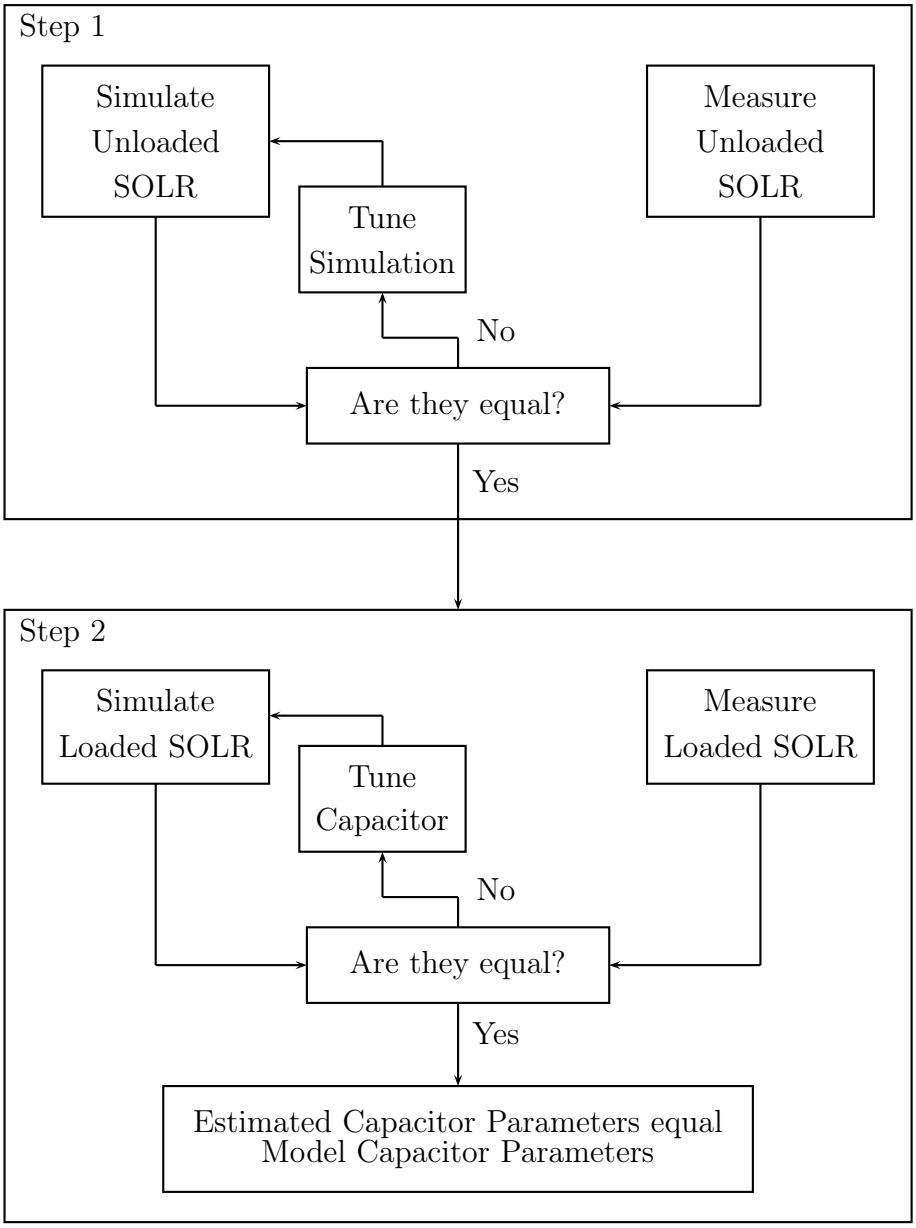

Figure 4.2: Simulation-based measurement process.

4.2 Capacitor Model

For the simulation experiments, capacitors from the ATC 600L 0402 family were used. Accurate models for these capacitors were provided by Modelithics, Inc. [28],

as were the models used in Chapter 3 to simulate the miniaturized filters. Though the specific details behind the models are proprietary, some of the theoretical background and modeling considerations can be found in [31]. For the sake of discussion the simpler model shown in Figure 4.3 will be used, where the factor F is nominally unity and will be used to vary the capacitor losses later on.

Figure 4.3: Simplified capacitor model.

As mentioned in the introduction, the conventional method using a high Q coaxial resonator presents some difficulties for small capacitors. Preliminary considerations show that for capacitors of size 0402 the error in ESR start increasing rapidly when the capacitance values are below 4 pF [30]. The high uncertainty prevents one from generating more accurate models, and the solution adapted so far is to assume that the ESR is the same for all the part values below ~ 3.9 pF. Figure 4.4 shows the modeled ESR against frequency for different capacitors from the ATC 600L 0402 family in a 60 mil Rogers 4003c substrate ($\varepsilon_r = 3.55$). Note how the ESR is the same for the capacitors smaller than 3.9 pF. It is important to remark that this is not actually the case in real capacitors, but a modeling compromise due to the lack of a measurement system that provides accurate values of ESR for small capacitors. In the rest of this chapter capacitors with nominal values of 0.5 pF, 1.0 pF, and 2.0 pF are used to explore the effect of ESR on the resonators quality factor.

In order to test the effect of the capacitors ESR on the quality factor of the resonators, the factor F from Figure 4.3 will be varied from 1, representing the nominal value, to 3 representing a 300% increase in the ESR value.

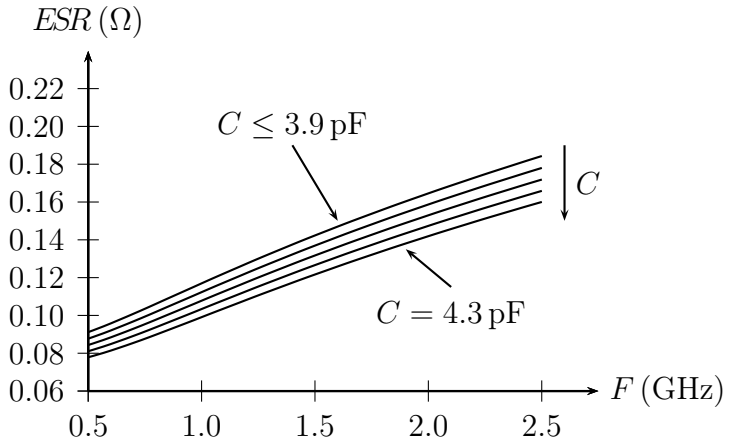

Figure 4.4: Modeled effective series resistance against frequency for capacitors with a nominal value below 4.3 pF belonging to the ATC 600L 0402 family.

4.3 Simulations and Results

The size of the square open loop resonators was designed to test the capacitors at 1 GHz and 2 GHz. As before, the substrate assumed was 60 mil Rogers 4003c with a loss tangent of $\tan\delta = 0.0027$. Table 4.1 summarizes the simulations that were performed. The last three columns of this table refer to the size of the resonators used; the parameters w, a_1, and a_2 are defined in Figure 4.5. Note that in order to produce a given center frequency for different capacitor values, the resonators must have different sizes.

Table 4.1: Matrix of simulations that were performed.

	Exp 1	Exp 2	Exp 3	Exp 4	Exp 5	Exp 6	Exp 7
Frequency (GHz)	1	1	1	1	2	2	2
Capacitance (pF)	0	0.5	1	2	0	0.5	1
Substrate	60 mil Rogers 4003c ($\varepsilon_r = 3.55$, $\tan\delta = 0.0027$)						
w (mm)	3	3	3	3	1.1	1.1	1.1
a_1 (mm)	26.4	21.8	18.2	13.6	13.2	7.2	5.6
a_2 (mm)	26.6	21.9	18.2	13.7	13.3	7.2	4.7

The results of the simulations at $f = 1$ GHz are presented on Figure 4.6. This comprises experiments two to four from Table 4.1. These results are congruent with

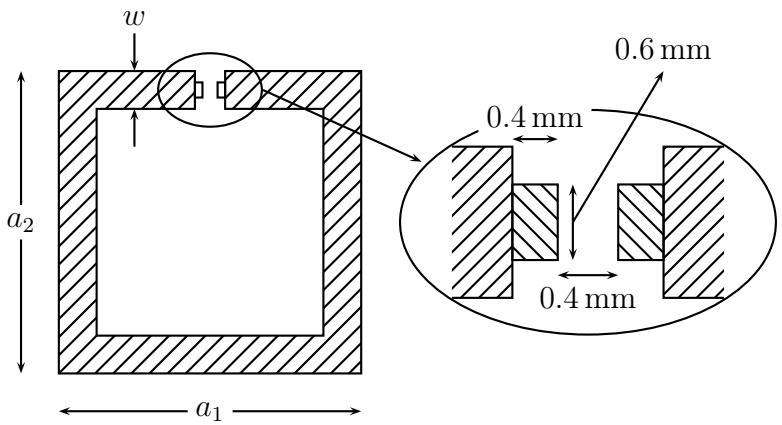

Figure 4.5: Resonator used

the observation stated previously that it is easier to measure the ESR of capacitors with high value. Observe, for instance, that the variation in the resonator Q is more dramatic for $C = 2\,\text{pF}$ than for $C = 0.5\,\text{pF}$. This means that the difficulty to measure the ESR to a given degree of accuracy increases with decreasing capacitance. What is remarkable from Figure 4.6 is that changes in the resonator Q due to changes in ESR would be reasonably easy to measure even for capacitors as small as 0.5 pF. Consider, as an example, a 1 pF capacitor with an estimated ESR found using conventional measurement techniques; if the actual ESR is 1.5 times larger than the estimated, that would produce a Q that is about 100 units below the expected value according to Figure 4.6(d). The results for $f = 2\,\text{GHz}$ are shown in Figure 4.7. The general trend is the same as in the 1 GHz case, but the absolute change in Q is more dramatic.

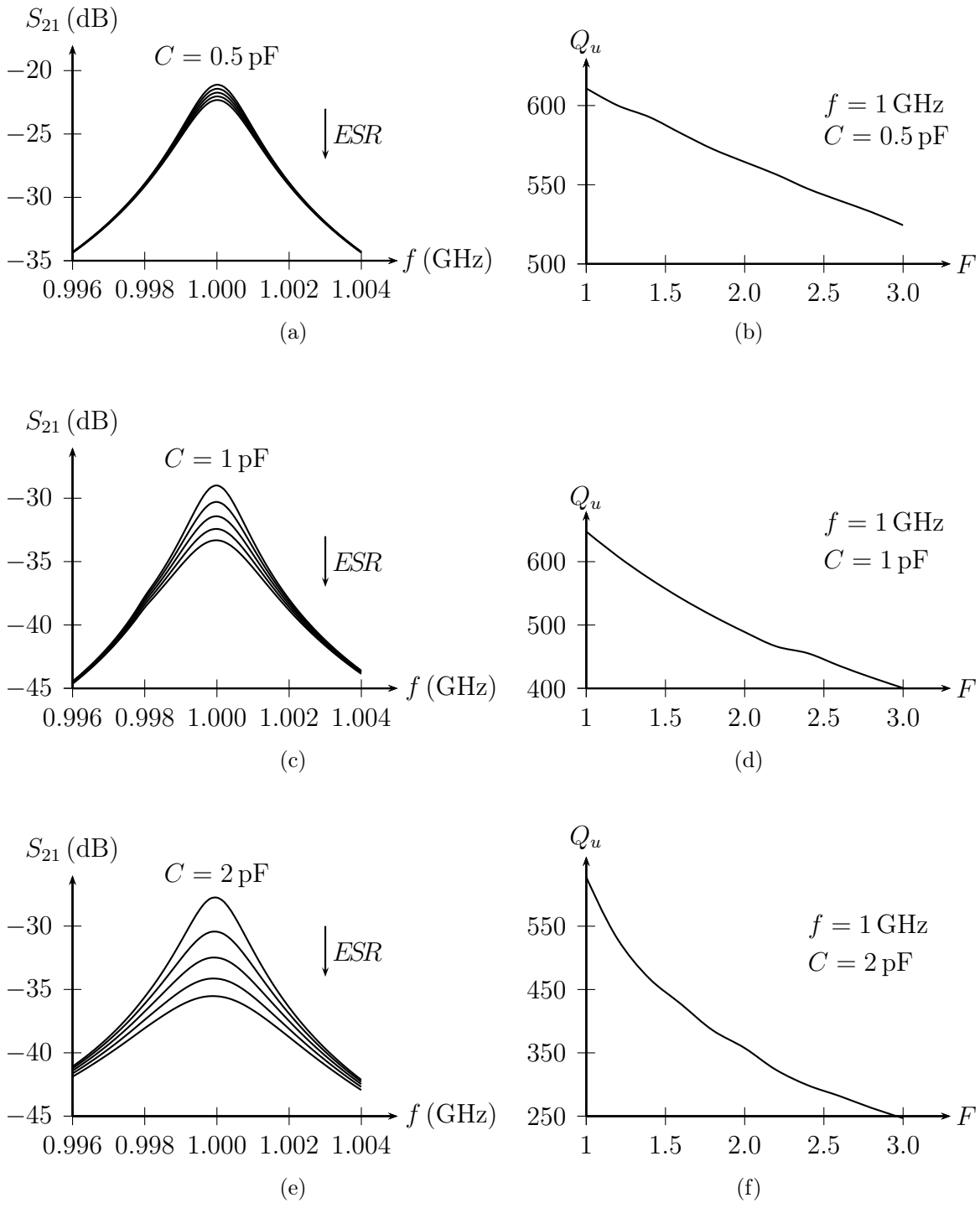

Figure 4.6: Transfer response and unloaded quality factor of different loaded resonators at 1 GHz. In all cases the transfer response is plotted for F varying uniformly between 1 and 3.

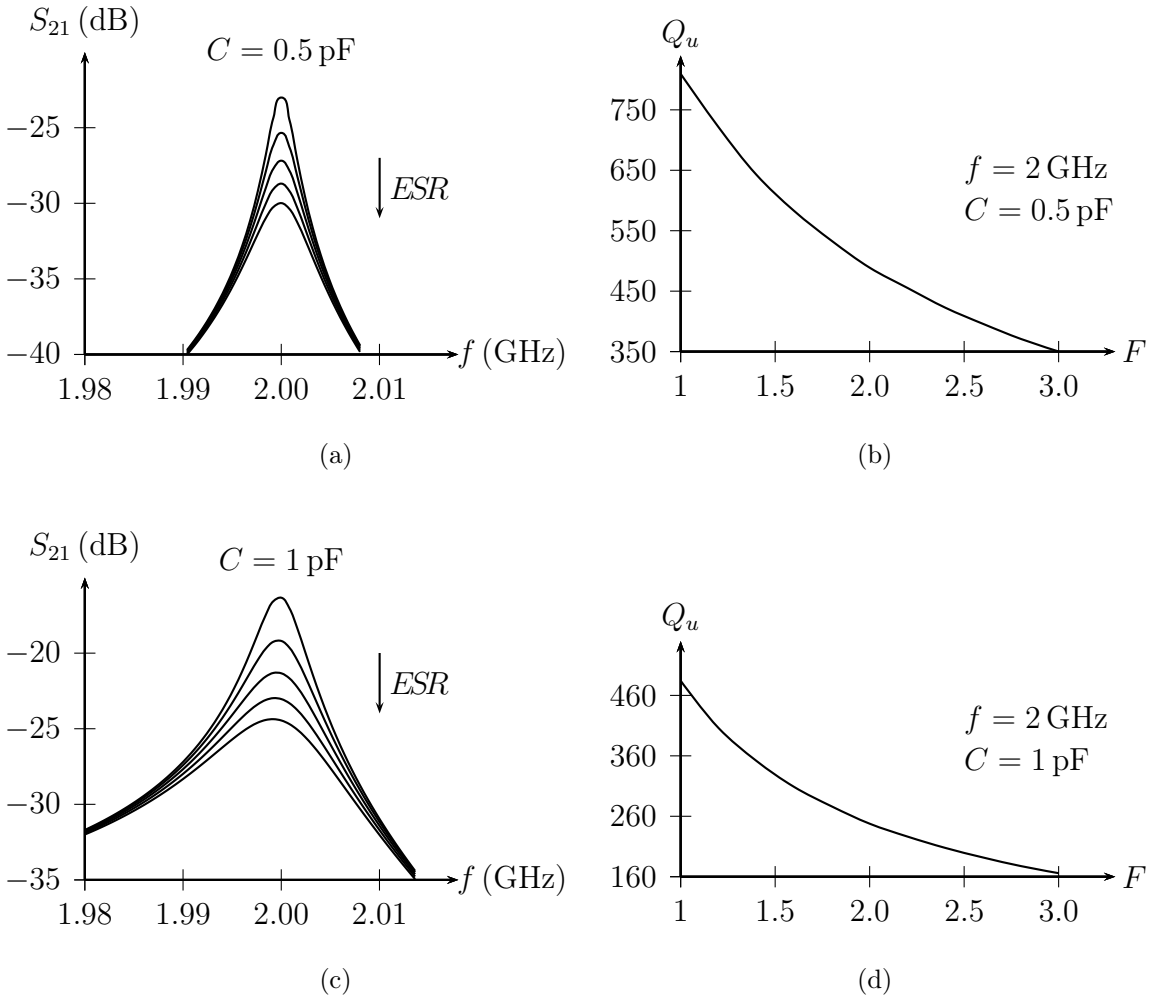

Figure 4.7: Transfer response and unloaded quality factor of different loaded resonators at 2 GHz. In all cases the transfer response is plotted for F varying uniformly between 1 and 3.

The results presented in this chapter are based on simulations only. In this scenario, even after considering the loss tangent of the substrate, the finite conductivity of the conductors, and radiation, the resonators presented a relatively high value of Q on the order of 350-400. The quality factor of the unloaded resonator plays an important part in its sensitivity to the capacitor ESR. If the quality factor is much smaller, the results presented previously are optimistic, and the actual variation of Q with F will be smaller.

In order to perceive the degree of discrepancy between simulation and measurement, an unloaded resonator was simulated, built, and measured. The result, shown in Figure 4.8, illustrates the point. Not only the Q is different, but the whole response is distinct throughout the band, and even the resonant frequency is off. The discrepancy could be caused by frequency dependent substrate parameters and anisotropy, and, to a lesser extent, mechanical tolerances. Different attempts were done to match the simulation to the measured response; the difference in Q can be accounted for by considering radiation loss, the roughness of the conductors, and increasing the loss tangent of the substrate. The challenge lies not in obtaining a set of these parameters that produce the measured Q, but in obtaining the right set that describes how the loss is physically distributed among these factors. For this purpose it is necessary to characterize the different loss mechanisms individually in the desired frequency band. Obtaining the right Q is necessary but may not be sufficient; matching accurately the response of the resonator throughout the whole band may require extracting properties of the substrate as the permittivity, including its dependency with frequency and anisotropy. It was found during this research that in order to match the responses shown in Figure 4.8, modifying all of these parameters may be necessary. A particular solution was found using a lossy and anisotropic substrate, however, the degree of anisotropy was exceedingly high and could not be trusted without further investigation.

As pointed out before, one way to deal with this issue would be to employ a well known substrate with tighter tolerances like Quartz, Teflon, or Alumina. These materials also have very low loss tangents being even more attractive for this application. In any case, the process of matching the simulation to the measurement should include the extraction of accurate substrate parameters at the desired frequency band

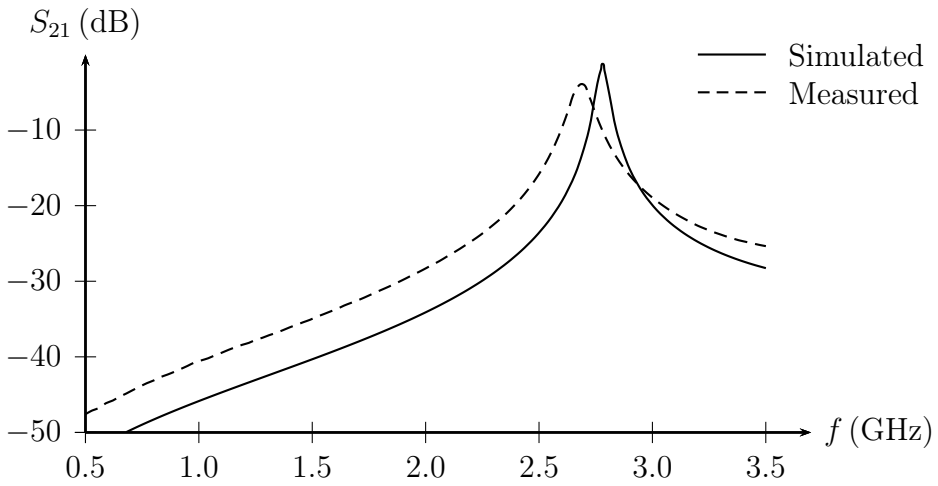

Figure 4.8: Measured and simulated unloaded square open loop resonator near 2.75 GHz.

instead of using the nominal values. The completion of this task was beyond the scope of this research.

As final comment, there is the question about why, if it is so difficult to obtain simulation results that closely match the measured data, it is still possible to design working devices based on such simulators. The reason is that for general engineering task, accurate match between measurements and simulation is not necessary. As an illustration consider the design of microstrip filters, if the system level specification for the minimum in-band return loss is 15 dB then usually the filter is designed for a return loss near 20 dB instead [25]. From an engineering point of view, computer simulations are extremely useful not because they produce exact results, but because, when used properly, can lead to first-pass design success.

Chapter 5

Conclusion

The miniaturization of microwave filters below 3 GHz remains an active area of research due to the relatively large physical size of traditional resonators and the great demand from the wireless communication industry within this band. One of the most popular structures for microstrip implementations is the square open loop resonator due to its compact size and versatility.

In this thesis a miniaturization technique was studied that is based on the loading of a square open loop resonator with a high Q capacitor. It was shown that this allows for a high degree of miniaturization with size reductions of more than 80% with respect to a conventional square open loop resonator filter. Moreover, the in-band response of the filter was not compromised by the miniaturization process, and the stop-band response was extended with a second pass-band higher than 4.5 times the center frequency.

The problem of estimating the effective series resistance of small capacitors at microwaves frequencies was also considered. It was proposed that the miniature square open loop resonator could be used to measure the ESR of the loading capacitor as long as an accurate model for the microstrip structure is obtained in advance.

5.1 Recommendations

Some subjects that could be studied further are:

- The possibility of designing cross-coupled filters using the miniaturization technique proposed herein. For this a different way of generating an electric-like coupling should be devised. A possibility could be to use a different input/output structure that allows for a phase reversing in the coupling of the first and last resonator for quadruplet sections. Another possibility could involve the use of multiple layers to achieve different kinds of couplings.

- A thorough study of a substrate in order to implement the method proposed in Chapter 4 to measured the capacitor of a small capacitor. The characterization could be made using a combination of simple test structures and existing methods to extract the radiation, conductor, and dielectric loss individually.

- The impact of the studied miniaturization technique for applications of the square open loop resonator other than filters. One example is the use of split ring resonators for meta-material applications. It was shown in Chapter 3 that the current distribution in the miniature resonator is almost constant along it; this may be advantageous since this resonators are used as artificial paramagnetic and diamagnetic materials.

References

[1] R. R. Mansour, "Filter technologies for wireless base stations," *IEEE Microwave Magazine*, vol. 5, no. 1, pp. 68–74, Mar. 2004.

[2] J. Hong, "Reconfigurable planar filters," *IEEE Microwave Magazine*, vol. 10, no. 6, pp. 73–83, Oct. 2009.

[3] M. Nisenoff and J. M. Pond, "Superconductors and microwaves," *IEEE Microwave Magazine*, vol. 10, no. 3, pp. 84–95, May 2009.

[4] J. Hong and M. Lancaster, "Canonical microstrip filter using square open-loop resonators," *Electronics Letters*, vol. 31, no. 23, pp. 2020–2022, Nov. 1995.

[5] ——, "Couplings of microstrip square open-loop resonators for cross-coupled planar microwave filters," *IEEE Transactions on Microwave Theory and Techniques*, vol. 44, no. 12, pp. 2099–2109, Dec. 1996.

[6] ——, "Microstrip cross-coupled trisection bandpass filters with asymmetric frequency characteristics," *IEE Proceedings on Microwaves, Antennas and Propagation*, vol. 146, no. 1, pp. 84–90, Feb. 1999.

[7] ——, "Design of highly selective microstrip bandpass filters with a single pair of attenuation poles at finite frequencies," *IEEE Transactions on Microwave Theory and Techniques*, vol. 48, no. 7, pp. 1098–1107, Jul. 2000.

[8] ——, "Compact microwave elliptic function filter using novel microstrip meander open-loop resonators," *Electronics Letters*, vol. 32, no. 6, pp. 563–564, Mar. 1996.

[9] ——, "Theory and experiment of novel microstrip slow-wave open-loop resonator filters," *IEEE Transactions on Microwave Theory and Techniques*, vol. 45, no. 12, pp. 2358–2365, 1997.

[10] S. Lee and C. Tsai, "New cross-coupled filter design using improved hairpin resonators," *IEEE Transactions on Microwave Theory and Techniques*, vol. 48, no. 12, pp. 2482–2490, 2000.

[11] J. Hong and M. Lancaster, "Recent advances in microstrip filters for communications and other applications," in *IEE Colloquium on Advances in Passive Microwave Components*. Iee, 2002, pp. 2–2.

[12] S. Park, K. V. Caekenberghe, and G. M. Rebeiz, "A miniature 2.1-ghz low loss microstrip filter with independent electric and magnetic coupling," *IEEE Microwave and Wireless Components Letters*, vol. 14, no. 10, pp. 496–498, Oct. 2004.

[13] J. Zhu and Z. Feng, "Microstrip interdigital hairpin resonator with an optimal physical length," *Microwave and Wireless Components Letters, IEEE*, vol. 16, no. 12, pp. 672–674, Dec. 2006.

[14] J. Hong, H. Shaman, and Y. Chun, "Dual-mode microstrip open-loop resonators and filters," *IEEE Transactions on Microwave Theory and Techniques*, vol. 55, no. 8, pp. 1764–1770, Aug. 2007.

[15] R. Mao, X. Tang, L. Wang, and G. Du, "Miniaturized hexagonal stepped-impedance resonators and their applications to filters," *IEEE Transactions on Microwave Theory and Techniques*, vol. 56, no. 2, pp. 440–448, Feb. 2008.

[16] J. Hong, "Recent progress in miniature microwave filters," in *Art of Miniaturizing RF and Microwave Passive Components, 2008. IMWS 2008. IEEE MTT-S International Microwave Workshop Series on*, no. Dec. IEEE, 2009, pp. 1–6.

[17] M. Sagawa, K. Takahashi, and M. Makimoto, "Miniaturized hairpin resonator filters and their application to receiver front-end MIC's," *IEEE Transactions on Microwave Theory and Techniques*, vol. 37, no. 12, pp. 1991–1997, 1989.

[18] M. Makimoto and M. Sagawa, "Varactor tuned bandpass filters using microstrip-line ring resonators," in *IEEE MTT-S Digest*, 1986.

[19] M. Dishal, "Alignment and adjustment of synchronously tuned multiple-resonant-circuit filters," *Proceedings of the IRE*, vol. 39, no. 11, pp. 1448–1455, Nov. 1951.

[20] K. Chang and L.-H. Hsieh, *Microwave ring circuits and related structures*. Wiley-IEEE, 2004.

[21] J. Hong and M. Lancaster, *Microstrip filters for RF/microwave applications*. John Wiley and Sons, 2001.

[22] E. Belohoubek and E. Denlinger, "Loss considerations for microstrip resonators (short papers)," *IEEE Transactions on Microwave Theory and Techniques*, vol. 23, no. 6, pp. 522 – 526, Jun. 1975.

[23] A. Gopinath, "Maximum Q-factor of microstrip resonators," *IEEE Transactions on Microwave Theory and Techniques*, vol. 29, no. 2, pp. 128 – 131, Feb. 1981.

[24] D. Kajfez, "Q factor measurements, analog and digital," 1999. [Online]. Available: http://www.ee.olemiss.edu/darko/rfqmeas2b.pdf

[25] D. Swanson, "Narrow-band microwave filter design," *IEEE Microwave Magazine*, vol. 8, no. 5, pp. 105–114, Oct. 2007.

[26] G. Matthaei, L. Young, and E. Jones, *Microwave Filters, Impedance-Matching Networks, and Coupling Structures*. Artech House, 1980.

[27] Sonnet em, Sonnet Software, North Syracuse, NY. [Online]. Available: www.sonnetsoftware.com

[28] Passive components CLR library, Modelithics, Tampa, FL. [Online]. Available: www.modelithics.com

[29] J. Maher, R. Jacobsen, and R. Lafferty, "High-frequency measurement of Q-factors of ceramic chip capacitors," *IEEE Transactions on Components, Hybrids, and Manufacturing Technology*, vol. 1, no. 3, pp. 257–264, Sep. 1978.

[30] T. Weller, private communication, December 2010.

[31] B. Lakshminarayanan, H. C. Gordon, and T. M. Weller, "A substrate-dependent CAD model for ceramic multilayer capacitors," *IEEE Transactions on Microwave Theory and Techniques*, vol. 48, no. 10, pp. 1687–1693, Oct. 2000.